A Comparison of Mixture Fraction Approaches for Coal Combustion Simulations

Andrew P. Richards, David O. Lignell, and Thomas H. Fletcher*

Chemical Engineering Department, Brigham Young University

Provo, Utah, USA 84602

Abstract

Simulations of industrial-scale coal combustion systems often use simplifying assumptions of gas-phase chemical reactions due to computational considerations and complications of turbulence-chemistry interactions. One common method is to use a mixture fraction approach combined with equilibrium chemistry, assuming that reactions are mixing-limited. Other assumptions may be that the gas from the coal may be assumed to have the same composition as the coal, or a simple compound like benzene, or that the char is assumed to have the chemical composition and heating value of graphite. This paper shows that these simplifying assumptions lead to inaccuracies in equilibrium temperature and gas-phase mole fractions, with the peak CO and H_2O mole fractions varying by up to 20 mol% and the peak equilibrium temperature varying by 200 K, depending on the initial fuel chosen. In addition, this paper explores the variability, accuracy, and utility of one-, two-, and three-fuel mixture fraction approaches to treat char, tar, and light gases.

Keywords:

Coal; Pyrolysis; Multiple Mixture Fractions; Equilibrium Modeling; Cantera; NASA-CEA

*Corresponding Author

1. Introduction

Large-scale simulations of coal combustion systems have become very important both to investigate new technologies and to increase understanding of coal combustion phenomena. Flexible and accurate submodels are necessary for the overall accuracy and utility of the simulation. Gas-phase reactions are an integral part of coal combustion simulations, and influence the bulk gas composition, local gas temperature, and can have implications on fluid flow, heat transfer, and mass transfer [1]. Simplifying assumptions are often used to decrease computational complexity, especially if computational resources are limited. Advances in computer technology allow for larger and more complex problems to be simulated, and larger and more complex submodels are becoming increasingly used to decrease overall error and uncertainty in these large-scale simulations [2, 3].

Coal is very complex, and the structure and composition change even in coals from the same seam [4]. Because of this complexity, many of the simplifying assumptions in gas-phase equilibrium of coal systems have dealt with simplifying coal-based fuel compositions, particularly the compositions of pyrolysis products (char, tar, and light gases). Frequently coal char is modeled as pure carbon with the thermochemical properties of either graphite [5-12] or of the parent coal [13-16]. This is perhaps useful in heterogeneous char reactions since oxidation and gasification reactions primarily target the carbon in the char. However, this approach falls short in calculating other combustion products (i.e., H_2O and other hydrogen-based products), since the char retains some hydrogen and other atoms such as oxygen, nitrogen, and sulfur [17, 18].

Other simulations have simplified the compositions and energies of the volatile species, often using one or more of several simple hydrocarbons in the place of the more complex tars

and other volatile gases. Some simulations use methane in the place of the total volatiles [7, 12, 14, 19-29] or other simple C_2 hydrocarbons [30]. Other approaches use a mix of common pyrolysis gases (CH_4, C_6H_6, CO, CO_2, H_2, N_2, H_2S, etc.) in variable quantities to ensure elemental balance between the original coal and gaseous species [20, 23, 31, 32]. Some even use constant generic hydrocarbon estimates ($C_xH_yO_z$) to better approximate volatile species [10, 13, 15, 24, 29, 33-35], often approximated using the composition of the original coal. While these simplified approaches may be appropriate for smaller-scale or simplified calculations, they may be inadequate for accurate large-scale simulations, especially since inaccuracies in CO_2 and H_2O gas compositions greatly affect other parts of the coal combustion system like radiative heat transfer [36]. Volatile gases released by coal pyrolysis reactions contain many of these simple hydrocarbons, but the total volatiles tend to be much more complex, particularly the tar species [18, 37]. This paper details attempts to quantify uncertainty and error in using these simplified approaches by comparing several of the simple coal surrogate gases to measured coal-based fuels.

Coal products change composition depending on a variety of conditions, including local gas temperature, particle residence times, and heating rate [17, 38, 39]. Compositions and other properties also change as a particle moves through the hot gas environment [40]. To help with mixing and variable fuel compositions, large-scale simulations frequently use one of several different modeling approaches, including flamelet and progress variables [11, 41-44], mixture fractions [3, 45-50], full equilibrium [51], approximations to equilibrium such as the water-gas shift reaction [52], detailed kinetic mechanisms of simpler hydrocarbon fuels such as GRI3.0 [21, 22, 41, 43, 53, 54], or even a combination of several different approaches [11, 27, 28, 44, 46].

This paper compares three different levels of mixture fraction analyses, including one, two, and three fuel mixture fractions for coal combustion scenarios. The one-mixture fraction approach assumes all mass originating in the coal has the same elemental composition and heating value as the parent coal and is the most common mixture fraction approach (e.g., [1, 3, 51, 55]). The two-mixture fraction approach treats volatiles and char compositions and heating values separately, and was explored by Flores and Fletcher [50] in simulations of three laboratory-scale coal combustors. In that study, the one- and two-mixture fraction approaches showed differences in calculated temperatures and species concentrations near the burner, especially with NO predictions. The three-mixture fraction approach treats light gas, tar, and char separately. These three approaches are compared in this paper using equilibrium calculations, rather than performing simulations of pilot- or industrial-scale furnaces. This simplified approach allows focus on the chemical state spaces, which can be widely explored, and which would be encompassed in specific furnace simulations.

1.1 Mixture Fractions

This section introduces the mixture fraction methods used in this analysis, beginning with a brief discussion on mixture fractions in general. This discussion includes some of the differences in applying mixture fractions to coal-based fuels as opposed to other simple hydrocarbon fuels. Next, each level of mixture fraction comparison is detailed, starting with the one-mixture fraction comparison, followed by the two-mixture fraction comparison. Finally, the three-mixture fraction comparison is discussed.

At its most simple definition, a mixture fraction analysis involves defining a reacting system (e.g., combustion of a hydrocarbon fuel with air) into two types of streams—one that

93 includes all fuels and another that includes the oxidizing gases. In most gas-phase combustion
94 reactions of simple hydrocarbon fuels, mixture fractions can be considered "conserved scalars,"
95 which means that the mixture fraction does not change with reacting conditions. Conserved
96 scalars simplify reacting flow calculations and can be anything from elemental mass fractions to
97 enthalpies of the different reacting streams, as long as it is a stream property that remains the
98 same throughout the reacting system [56]. This approach is a simple way to track material when
99 it mixes and reacts to equilibrium.

100 Mixture fractions in coal-based systems are not usually considered conserved scalars
101 because the mixture fractions typically include a separate source term to describe the addition of
102 material into the gas phase from a solid coal particle [1, 50]. This source term is necessary
103 because coal combustion is not a homogeneous reaction that occurs only in the gas phase, but
104 instead involves a complex reaction between a solid coal particle and other background gases
105 [4]. While using a source term is helpful in describing the physical processes of a coal
106 combustion reaction, it can complicate transport and reaction equations, making a mixture
107 fraction description of coal combustion difficult to incorporate into large-scale simulations.

108 The mixture fraction comparisons used in this paper are slightly different from those used
109 traditionally in simple hydrocarbon reactions and from previous work on coal-gas mixture
110 fractions. For this reason, a detailed derivation of the mixture fraction and other necessary
111 equations is detailed here. While there are multiple ways of defining a mixture fraction,
112 including the widely used Bilger's mixture fraction [57-59], this analysis explores two main
113 types of mixture fractions. The first is a more traditional form of mixture fraction (named here as
114 a "component" or "fuel" mixture fraction and labeled as f_i to avoid confusion with other mixture
115 fractions) which is the mass fraction of material originating in each stream. This component

mixture fraction, f_i, is calculated by dividing the mass of one fuel stream by the total mass of the mixture [56], shown in general form in Equation 1:

$$f_i = \frac{M_i}{M_{ox}+\sum_{i=1}^{N} M_i} \quad (1)$$

where f_i is the component mixture fraction of component i (coal, char, tar, oxidizer, etc.), M_i is the total mass of component i, M_{ox} is the total mass of the oxidizer component (e.g., air), and N indicates the total number of fuel components. The sum of all component mixture fractions adds to one, and the total number of fuel mixture fractions to completely describe a reacting system is $N-1$.

The component mixture fraction is commonly used to describe a system of one fuel stream and one oxidizer stream—otherwise known as a one-mixture fraction system. While one-mixture fraction systems are common with many types of gas-phase combustion applications, this type of component mixture fraction can be extended to two, three, or even more [60].

The second type of mixture fraction is called the "elemental" mixture fraction and labeled as Z_j to distinguish from the component mixture fraction. This type of mixture fraction describes the total mass fraction of each element in the reacting system [59, 61]. The elemental mixture fraction is shown in Equation 2:

$$Z_j = W_j \sum_{i=1}^{N} \frac{a_{ij} Y_i}{W_i} \quad (2)$$

where Z_j is the elemental mixture fraction of element j (i.e. carbon, hydrogen, etc.), W_j is the molecular weight of element j, W_i is the molecular weight of component i (including oxidizer

and all fuels), Y_i is the mass fraction of component i (the component mixture fraction), and a_{ij} is the number of atoms of element j in component i (for example, a sample fuel of benzene, C_6H_6 would have an a_{ij} of 6 for both carbon and hydrogen). In most simple hydrocarbon combustion systems, the total number of primary elements is four (CHON), however, in coal combustion applications, sulfur is present, leading to five total elemental mixture fractions to describe the primary organic elements (CHONS) present in the fuel and oxidizer streams. Like the component mixture fraction, the elemental mixture fractions sum to one.

Another useful parameter in combustion modeling is the equivalence ratio [56] (shown in Equation 3), which relates the fuel-to-oxidizer ratio of a mixture to the fuel's stoichiometric fuel-to-oxidizer ratio.

$$\phi_i = \frac{\frac{n_i}{n_{ox}}}{\left(\frac{n_i}{n_{ox}}\right)_{stoich}} \tag{3}$$

where ϕ_i is the equivalence ratio of fuel i, n_i is the number of moles of fuel i, n_{ox} is the moles of oxidizer (i.e., air), and the subscript $stoich$ is the oxidizer-to-fuel ratio at stoichiometric proportions. The equivalence ratio or component mixture fraction can be used to determine the total moles of oxidizer in the system if the amount of fuel is fixed to a constant value.

1.1.1 One-Mixture Fraction Comparison

A one-mixture fraction method divides a combustion mixture into two streams—one fuel stream and one oxidizer stream. This is a common method used in simple hydrocarbon combustion applications and has also been applied to coal-gas mixtures [1]. The one-mixture

fraction comparison is the simplest of the three detailed here. In coal systems, one mixture fraction is used to describe all gas from a raw coal mixing with the oxidizing gas. Coal gas is a mixture of a large number of different species with a wide variety of composition and energy properties. The fuel mixture fraction (as shown generally in Equation 1) of a one-mixture fraction system is shown in Equation 4:

$$f = \frac{M_1}{M_0 + M_1} \tag{4}$$

where f is the fuel mixture fraction (coal or any number of coal surrogate gases), M_0 is the mass of the oxidizer stream, and M_1 is the mass of the fuel stream. The mass fraction of any element in the system can be found using the elemental mass fractions (shown generally in Equation 2), as shown in the Equations 5 to 9 (in order of CHONS):

$$Z_C^1 = W_C \left(\frac{a_{C,1} f}{W_1} + \frac{a_{C,0}(1-f)}{W_0} \right) \tag{5}$$

$$Z_H^1 = W_H \left(\frac{a_{H,1} f}{W_1} + \frac{a_{H,1}(1-f)}{W_0} \right) \tag{6}$$

$$Z_O^1 = W_O \left(\frac{a_{O,1} f}{W_1} + \frac{a_{O,0}(1-f)}{W_0} \right) \tag{7}$$

$$Z_N^1 = W_N \left(\frac{a_{N,1} f}{W_1} + \frac{a_{N,0}(1-f)}{W_0} \right) \tag{8}$$

$$Z_S^1 = W_S \left(\frac{a_{S,1} f}{W_1} + \frac{a_{S,0}(1-f)}{W_0} \right) \tag{9}$$

where Z_C^1 is the elemental mixture fraction of carbon in a one-mixture fraction system (denoted by superscript 1), W_C is the molecular weight of carbon, $a_{C,1}$ is the number of atoms of carbon in

the fuel stream (estimated using the mole fraction of carbon in the case of coal-based fuels), f is the fuel mixture fraction (mass fraction of fuel), and W_1 is the molecular weight of the fuel stream. Similar variables are used for each element, with a subscript of zero used to denote properties of the oxidizer stream added to the elemental mixture fractions of oxygen and nitrogen (the two elements that are in the oxidizer stream). These are generalized equations, but for a typical coal combustion application, the elemental mixture fractions would be simpler. Air does not typically include any carbon, hydrogen, or sulfur, so the $a_{i,0}$ values (e.g., $a_{C,0}$) for each of those elements would be zero. These values would be different if different oxidizer gases were used (e.g., oxy-fuel combustion). Because there is only one fuel stream, only one equivalence ratio (shown generally in Equation 3) is needed to describe this system. The one-mixture fraction equivalence ratio is shown in Equation 10.

$$\phi = \frac{\frac{n_1}{n_0}}{\left(\frac{n_1}{n_0}\right)_{stoich}} \tag{10}$$

where subscripts of zero and one are again used to denote the moles of the oxidizer and fuel streams, respectively.

1.1.2 Two-Mixture Fraction Comparison

A two-mixture fraction system is a little more complex than a one-mixture fraction system. Instead of only using a single fuel stream, a two-mixture fraction system includes two fuel streams. While a two-mixture fraction method does not usually provide any benefit for simple hydrocarbon combustion reactions, these methods can benefit coal combustion reactions since pyrolysis and char combustion occur on different time scales. Coal reaction products can

therefore be treated as volatile gases (named the total volatiles) and the solid that remains after pyrolysis (named the char). These two general categories of pyrolysis products comprise the two fuel streams of a two-mixture fraction system. These two fuel mixture fractions are described in Equations 11 and 12.

$$f_1 = \frac{M_1}{M_0+M_1+M_2} \tag{11}$$

$$f_2 = \frac{M_2}{M_0+M_1+M_2} \tag{12}$$

where the oxidizer stream is again denoted with a zero subscript, and subscripts of 1 and 2 are used to denote the mass and mixture fractions of the char and volatiles streams, respectively. Like all mixture fractions here, f_1 and f_2 sum to one minus the oxidizer mixture fraction (f_0). The mass fractions of the major elements in the combustion system can again be calculated using the elemental mixture fractions in Equations 13 to 17.

$$Z_C^2 = W_C\left(\frac{a_{C,1}f_1}{W_1} + \frac{a_{C,2}f_2}{W_2} + \frac{a_{C,0}(1-f_1-f_2)}{W_0}\right) \tag{13}$$

$$Z_H^2 = W_H\left(\frac{a_{H,1}f_1}{W_1} + \frac{a_{H,2}f_2}{W_2} + \frac{a_{H,0}(1-f_1-f_2)}{W_0}\right) \tag{14}$$

$$Z_O^2 = W_O\left(\frac{a_{O,1}f_1}{W_1} + \frac{a_{O,2}f_2}{W_2} + \frac{a_{O,0}(1-f_1-f_2)}{W_0}\right) \tag{15}$$

$$Z_N^2 = W_N\left(\frac{a_{N,1}f_1}{W_1} + \frac{a_{N,2}f_2}{W_2} + \frac{a_{N,0}(1-f_1-f_2)}{W_0}\right) \tag{16}$$

$$Z_S^2 = W_S\left(\frac{a_{S,1}f_1}{W_1} + \frac{a_{S,2}f_2}{W_2} + \frac{a_{S,0}(1-f_1-f_2)}{W_0}\right) \tag{17}$$

where Z_C^2 is the elemental mixture fraction of carbon in a two-mixture fraction system (note, the superscript 2 does not indicate a squared value, only that the elemental mixture fraction describes that of a two-mixture fraction system), and the other variables are extensions of those previously described. Like the one-mixture fraction comparison, the five elemental mixture fractions sum to one and would simplify based on the oxidizer gases used. In addition to the two fuel mixture fractions, there are also two independent equivalence ratios that can be used to determine the amount of oxidizer in the system, shown in Equations 18 and 19.

$$\phi_1 = \frac{\frac{n_1}{n_0}}{\left(\frac{n_1}{n_0}\right)_{stoich}} \tag{18}$$

$$\phi_2 = \frac{\frac{n_2}{n_0}}{\left(\frac{n_2}{n_0}\right)_{stoich}} \tag{19}$$

with subscripts of 0, 1, and 2 describing the moles of oxidizer, char, and volatiles, respectively.

1.1.3 Three-Mixture Fraction Comparison

The three-mixture fraction comparison adds a third fuel mixture fraction. Like the two-mixture fraction comparison, three mixture fractions generally are not useful in most simple hydrocarbon combustion applications. Coal combustion systems, however, might benefit from three mixture fractions. When coal reacts, the total volatiles can be further divided into two additional categories: tars (volatile gases that condense to a sticky liquid at room temperature) and light gases (volatile gases that remain as gas at room temperature). This leads to three total fuel streams—one for the char, one for the tar, and a third for the light gases. The three fuel streams are described by three fuel mixture fractions, shown in Equations 20 to 22:

$$f_1 = \frac{M_1}{M_0+M_1+M_2+M_3} \quad (20)$$

$$f_2 = \frac{M_2}{M_0+M_1+M_2+M_3} \quad (21)$$

$$f_3 = \frac{M_3}{M_0+M_1+M_2+M_3} \quad (22)$$

where a subscript of zero again describes the oxidizer stream values, a subscript of 1 corresponds to the char stream, a subscript of 2 details the tar stream, and a subscript of 3 indicates the light gas stream. All three fuel mixture fractions and the oxidizer mixture fraction (f_0) again sum to 1. The mass fractions of each element in the mixture can again be found by calculating the elemental mixture fractions, in Equations 23 to 27:

$$Z_C^3 = W_C\left(\frac{a_{C,1}f_1}{W_1} + \frac{a_{C,2}f_2}{W_2} + \frac{a_{C,3}f_3}{W_3} + \frac{a_{C,0}(1-f_1-f_2-f_3)}{W_0}\right) \quad (23)$$

$$Z_H^3 = W_H\left(\frac{a_{H,1}f_1}{W_1} + \frac{a_{H,2}f_2}{W_2} + \frac{a_{H,3}f_3}{W_3} + \frac{a_{H,0}(1-f_1-f_2-f_3)}{W_0}\right) \quad (24)$$

$$Z_O^3 = W_O\left(\frac{a_{O,1}f_1}{W_1} + \frac{a_{O,2}f_2}{W_2} + \frac{a_{O,3}f_3}{W_3} + \frac{a_{O,0}(1-f_1-f_2-f_3)}{W_0}\right) \quad (25)$$

$$Z_N^3 = W_N\left(\frac{a_{N,1}f_1}{W_1} + \frac{a_{N,2}f_2}{W_2} + \frac{a_{N,3}f_3}{W_3} + \frac{a_{N,0}(1-f_1-f_2-f_3)}{W_0}\right) \quad (26)$$

$$Z_S^3 = W_S\left(\frac{a_{S,1}f_1}{W_1} + \frac{a_{S,2}f_2}{W_2} + \frac{a_{S,3}f_3}{W_3} + \frac{a_{S,0}(1-f_1-f_2-f_3)}{W_0}\right) \quad (27)$$

where Z_C^3 describes the elemental mixture fraction of carbon in a three-mixture fraction system (denoted by a superscript 3, note that this does not indicate a cubed value), and the remaining variables are likewise extensions of those described in the one- and two-mixture fraction comparisons. Additionally, there are three independent equivalence ratios in a three-mixture fraction system:

$$\phi_1 = \frac{\frac{n_1}{n_0}}{\left(\frac{n_1}{n_0}\right)_{stoich}} \quad (28)$$

$$\phi_2 = \frac{\frac{n_2}{n_0}}{\left(\frac{n_2}{n_0}\right)_{stoich}} \quad (29)$$

$$\phi_3 = \frac{\frac{n_3}{n_0}}{\left(\frac{n_3}{n_0}\right)_{stoich}} \quad (30)$$

1.2 Equilibrium Programs

Two widely-used chemical equilibrium programs for combustion systems are used here: the stand-alone version of the NASA-CEA program [62, 63] and the Python interface of Cantera [64]. Both programs calculate equilibrium states based on an input of initial conditions, including chemical and thermodynamic properties of reactants, relying primarily on Gibbs free energy minimization. Both programs also use similar thermodynamic property models with polynomial representations of heat capacity, enthalpy, and entropy states of chemical species. Additionally, both programs calculate an adiabatic equilibrium temperature, which can be used as a comparison between fuels, however, real combustion systems are never truly adiabatic. Large-scale simulations would take this into account by including a heat loss term. The NASA code is not set up to deal with any heat loss in a real system, however, Cantera is flexible enough that it could be used in conjunction with stand-alone research codes that adequately address heat loss concerns.

The NASA-CEA program has been used to calculate equilibrium states of all types of fuels, including solid fuels. In order to equilibrate coal systems, some novel subroutines were developed to create Cantera mechanism files for coal-like fuels. These subroutines use the elemental composition, enthalpy of formation, and the reference temperature at which the

289 enthalpy of formation is calculated. These inputs were used to develop coefficients for the
290 polynomial thermodynamic property models. Finally, the thermodynamic coefficients and other
291 relevant information were included in a mechanism file. These subroutines can be applied to
292 calculate the Cantera mechanism files for any coal-based fuels. Some instabilities were observed
293 in Cantera equilibrium calculations when just the coal mechanism files were used. To eliminate
294 these instabilities, the Cantera mechanism for solid carbon (graphite) had to be introduced along
295 with mechanism files for the unreacted coal (or other solid fuel) and combustion/background
296 gases. Additional mechanism files were created for the coal surrogate and combustion gases.
297 A second subroutine was created around the Cantera solver to iterate over the range of
298 equivalence ratios for each fuel stream. The mixture fractions were calculated at each
299 equivalence ratio and for each equilibrium state. The additional subroutine made the Cantera
300 calculations more convenient, especially for the two- and three-mixture fraction comparisons.
301
302 1.3 Experimental Data
303 Experimental data were gathered from several sources based on the following criteria:
304 (a) reported elemental compositions must be reported on a dry, ash-free (DAF) basis or enough
305 information provided to calculate the elemental compositions on a DAF basis; (b) heating values
306 (enthalpies of combustion) must be reported on a DAF basis, or enough information provided to
307 calculate them on a DAF basis; (c) comparisons using two mixture fractions must have average
308 elemental compositions and heating values for both char and either tar or total volatiles; and (d)
309 data for the three-mixture fraction comparison must have enough information to calculate
310 elemental compositions and heating values for coal char, tar, and light gas. A review of a large
311 set of experimental heating values was reported by Richards, et al. [65], and all coal-based fuels

312 are taken from that data set. Some common coal surrogate gases are also used here. All fuels
313 used, along with their respective sources, are described in Table 1.
314
315 Table 1. Fuels used in this analysis

Fuel No.	Fuel Name	Source	Coal Rank
F-1	Graphite	Perry's Handbook [66]	N/A
F-2	Benzene	Perry's Handbook [66]	N/A
F-3	Methane	Perry's Handbook [66]	N/A
F-4	Ethane	Perry's Handbook [66]	N/A
F-5	Ethylene	Perry's Handbook [66]	N/A
F-6	Pittsburgh #8 (Pitt 8) Coal	Proscia et al. [67]	HVA
F-7	Lower Kittanning Coal	Proscia et al. [67]	LVB
F-8	Millmerran Coal	Edwards et al. [68]	Subbituminous
F-9	Liddell Coal	Edwards et al. [68]	Bituminous
F-10	Mammoth Seam Coal	Miller [69]	Anthracite
F-11	Beulah Zap Coal	Miller [69]	Lignite
F-12	Buck Mountain Coal	Miller [69]	Anthracite
F-13	#8 Leader Seam Coal	Miller [69]	Anthracite
F-14	#8 Seam Coal	Miller [69]	Semi-anthracite
F-15	Gunnison Coal	Miller [69]	Semi-anthracite
F-16	L. Spadra Seam Coal	Miller [69]	Semi-anthracite

316

All 16 fuels were used in the one-mixture fraction comparison, with fewer in the two-mixture fraction comparison, and only one used (F-6, Pitt 8) in the three-mixture fraction comparison. The fuel cases for each mixture fraction analysis are described in the Results and Discussion section.

While the elemental compositions and heating values of most of the fuels listed in Table 1 can be found in Richards, et al [65], a brief summary of some of the compositional differences between the fuels used here is warranted. Table 2 shows the DAF wt% of carbon, hydrogen, oxygen, nitrogen, and sulfur for a few of the coal-based fuels. This table is to illustrate some of the compositional differences that occur between different coal-based fuels, including different coals, chars, and tars.

Table 2. Summary of Elemental Composition of Some Coal-Based Fuels

Fuel No.	Fuel Name	C	H	O	N	S
F-6	Pitt 8 Coal	82.36	5.51	8.56	1.65	1.92
F-6a	Pitt 8 Char	83.01	5.24	8.23	1.68	1.84
F-6b	Pitt 8 Tar	85.02	6.40	5.68	1.63	1.27
F-6c	Pitt 8 Volatiles	78.65	7.05	10.47	1.48	2.35
F-6d	Pitt 8 Light Gases	49.18	10.06	32.66	0.78	7.32
F-8	Millmerran Coal	78.40	6.70	13.10	1.20	0.60
F-11	Beulah Zap Coal	73.10	4.50	20.60	1.00	0.80
F-12	Buck Mountain Coal	90.80	2.60	5.20	0.80	0.60

Different coals and coal-based fuels have very different compositions, and this affects the compositions of combustion gases at equilibrium. The coal surrogate gases vary even more, with none having any oxygen, nitrogen, or sulfur as part of the fuel.

2. Approach

The one-mixture fraction analysis used both the Cantera and NASA-CEA programs. The NASA code is trusted in the coal community for evaluating equilibrium states of coal-based fuels, so it is used to evaluate Cantera as a viable alternative for calculating equilibrium states. Both equilibrium programs require similar inputs depending on if the fuel is included in the program data or is user-defined. Simple fuels are included in the NASA-CEA code and are directly available to Cantera via provided mechanism files; these include all five of the surrogate gases: graphite (carbon solid), benzene, methane, ethane, and ethylene. These simple fuels include all the composition and thermochemical properties required for the respective equilibrium programs. User-defined compounds need two main parameters for both programs: elemental composition (CHONS, on either a mass or mole basis) and an enthalpy (or heat) of formation. For most coal-based fuels, elemental compositions and heats of combustion (also called heating values) are reported for each fuel. Heats of formation can then be calculated for each fuel by converting from heating values by assuming complete combustion, as shown in Equations 31-33.

$$C_a H_b O_c N_d S_e = \alpha O_2 \rightarrow aCO_2 + \frac{b}{2} H_2O + \frac{d}{2} N_2 + eSO_2 \quad (31)$$

$$\alpha = a + \frac{b}{2} - \frac{c}{2} + e \quad (32)$$

$$\Delta H_r = \left(\sum_{i=1}^{n} \nu_i \Delta H_{i,f}\right)_{prod} - \left(\sum_{i=1}^{n} \nu_i \Delta H_{i,f}\right)_{react} \quad (33)$$

where a, b, c, d, and e are average molar compositions of the fuel, α is the stoichiometric amount of oxygen needed for complete combustion, ΔH_r is the enthalpy of reaction (also called heating value), ν_i is a generic stoichiometric coefficient of compound i, $\Delta H_{i,f}$ is the enthalpy of formation of compound i, subscripts $prod$ and $react$ designate properties of the products (CO_2, H_2O, etc.) and reactants (fuel and O_2), respectively.

In addition to supplying the equilibrium programs with the properties of each fuel, the mass or moles of each stream is necessary to complete equilibrium calculations. The NASA-CEA code allows the input of a list of equivalence ratios, which makes calculating the equilibrium states using NASA-CEA more convenient. Cantera needs the total amount of oxidizer, which can be calculated either using the equivalence ratio or fuel mixture fraction. Equilibrium calculations using the one-mixture fraction approach were performed for a range of equivalence ratios from 0.1 (fuel-lean) to 3 (fuel-rich), with a greater number of points around the stoichiometric point (equivalence ratio of 1). The one-mixture fraction comparison used this equivalence ratio range to calculate the total air necessary to calculate equilibrium states for each fuel.

The procedure became more complicated with the two- and three-mixture fraction analyses. Because the analysis used a range of equivalence ratios rather than mixture fractions to determine the appropriate amounts of air for each fuel, a separate "mixing condition" was needed to determine the ratio of the fuel streams and fully define the system. If the fuel mixture fraction was used instead of the equivalence ratio, this fuel mixing condition would not be necessary. This fuel mixing condition is simply how much of each fuel stream is present prior to mixing with the oxidizer stream. The fuel mixing condition is allowed to vary between 0 and 1, with the sum of the fuel stream percentages not exceeding one.

In a two-mixture fraction system, there are two extremes in defining the fuel streams: (a) pure fuel 1 (char) with no fuel 2 (volatiles) and (b) pure fuel 2 (volatiles) with no fuel 1 (char). The first extreme would be defined as a fuel mixing condition of 0, which means that the fuel in the fuel mixture would only consist of fuel 1 (char) and the other extreme would correspond to a fuel mixing condition of 1, or 100 percent volatiles in the fuel. To span this fuel mixing space, five main fuel mixing cases were created with fuel ratios corresponding to 0, 25, 50, 75, or 100% volatiles (called Y_{vol}). This means that at 0% volatiles, the fuel is 100% char and vice-versa. Additionally, the reported pyrolysis yield for each fuel was used as a sixth fuel mixing ratio (between 10 and 60% depending on the fuel and pyrolysis conditions). Air was added to each fuel stream to vary the equivalence ratio independently between 0.1 and 3, with the total amount of oxidizer being a combination of the two equivalence ratios. This procedure was followed for all six fuel mixing ratios.

The three-mixture fraction comparison was slightly more complex, but a similar procedure to the two-mixture fraction comparison was followed to span the three-mixture fraction fuel mixing space. The three fuel streams (char, tar, and light gas) were allowed to vary among the same six values as the two-mixture fraction comparison (i.e., 0, 25, 50, 75, and 100%, and the reported pyrolysis yield of char, tar, and light gas). There are, however, two constraints placed on these fractions: (a) the three fuel fractions sum to one and (b) all fuel fractions must be between 0 and 1 (no negative numbers). Air was added to each fuel stream to vary the equivalence ratio between 0.1 and 3 for each fuel stream independently. The total amount of air is calculated for each fuel mixing condition and equivalence ratio. This procedure generated six total fuel mixing conditions for each two-mixture fraction comparison and 21 for each three-mixture fraction comparison.

Using the elemental compositions and enthalpies of formation for each fuel, and setting the pressure to one atmosphere, the equilibrium programs calculate the compositions of a large number of combustion gases for each equilibrium state. This analysis used six key variables from each equilibrium state to compare between fuels and mixture fraction methods: temperature and the mole fractions of O_2, CO_2, CO, H_2O, and graphite (i.e., solid carbon). This equilibrium temperature is an adiabatic temperature and does not account for any heat loss that might be observed in any real-world combustion applications.

Several statistical parameters [40, 65] were used to quantify error between the equilibrium states calculated by both NASA-CEA and Cantera, however, only one is presented here: the root-mean-square error (RMSE), found in Equation 7. The remainder of the statistical parameters and their results are discussed in Richards [70].

$$RMSE = \left(\frac{1}{N}\sum_{n=1}^{N}(\hat{y}_n - y_n)^2\right)^{\frac{1}{2}} \tag{34}$$

where y_n is the "true" value, $\hat{y}_n$ is the "questioned value", N is the total number of points in the comparison set. The equation for RMSE is a statistical parameter where experimentally observed and model prediction values are generally used in place of the "true" and "questioned" values, respectively. Both NASA and Cantera give predicted values for equilibrium states, so in order to adequately compare NASA to Cantera, in this analysis the NASA values are considered to be the "true" values and the Cantera are the "questioned" values. This distinction is not as important with the RMSE, however, it does make a slight difference in other statistical parameters (see Richards [70].

3. Results and Discussion

The results are discussed based on the number of fuel mixture fractions considered, starting with the one-mixture fraction comparison, followed by the two-mixture fraction comparison, and finally the three-mixture fraction approach compared to the one- and two-mixture fraction approaches. Each section consists of a description of the fuels used for each case. After the results are presented and discussed, a final section summarizes the key findings and discusses application to physical processes. Additional details and discussion are found in Richards [70].

3.1 One Mixture Fraction

The one-mixture fraction approach breaks the components into one fuel stream (e.g., coal) and one oxidizer stream (air). These two streams are mixed in different proportions according to the equivalence ratio. The fuels used in the one-mixture fraction analysis are listed in Table 3.

Table 3. One-Mixture Fraction Fuel Cases

Case Number	Fuel Number	Fuel Name	Coal Rank
1-1	F-1	Graphite	N/A
1-2	F-2	Benzene	N/A
1-3	F-3	Methane	N/A
1-4	F-4	Ethane	N/A
1-5	F-5	Ethylene	N/A
1-6	F-6	Pitt 8 Coal	HVA

1-7	F-6a	Pitt 8 Char	HVA, char
1-8	F-6b	Pitt 8 Tar	HVA, tar
1-9	F-7	Lower Kittanning Coal	LVB
1-10	F-8	Millmerran Coal	Subbituminous
1-11	F-9	Liddell Coal	Bituminous
1-12	F-10	Mammoth Coal	Anthracite
1-13	F-11	Beulah Zap Coal	Lignite
1-14	F-12	Buck Mountain Coal	Anthracite
1-15	F-13	#8 Leader Seam Coal	Anthracite
1-16	F-14	#8 Seam Coal	Semi-anthracite
1-17	F-15	Gunnison Coal	Semi-anthracite
1-18	F-16	L. Spadra Seam Coal	Semi-anthracite

Two main questions were addressed in the one-mixture fraction comparison: (1) how closely do the results from the NASA-CEA and Cantera programs compare to each other; and (2) what is the difference between the various coal surrogates and several different coal types? The comparison between the NASA and Cantera programs is briefly discussed first followed by a comparison of the different cases from Table 3.

3.1.1 NASA-CEA vs Cantera

The NASA equilibrium code has been widely used in the coal community over the years and is considered a standard in coal equilibrium calculations, but Cantera offers flexibility that

makes its integration into existing codes beneficial for large-scale simulations. This study was therefore performed to determine how closely the Cantera results align with the NASA results.

Both Cantera and NASA-CEA were used to calculate equilibrium states for all fuel cases listed in Table 3, comparing temperature and the mole fractions of O_2, CO_2, CO, H_2O, and graphite (solid carbon). Figure 1 shows the root-mean-square error (RMSE) between the NASA and Cantera results (additional error analysis is given by Richards [70]). Note that this is the RMSE over the entire range of equivalence ratio ranging from 0.1 to 3.0.

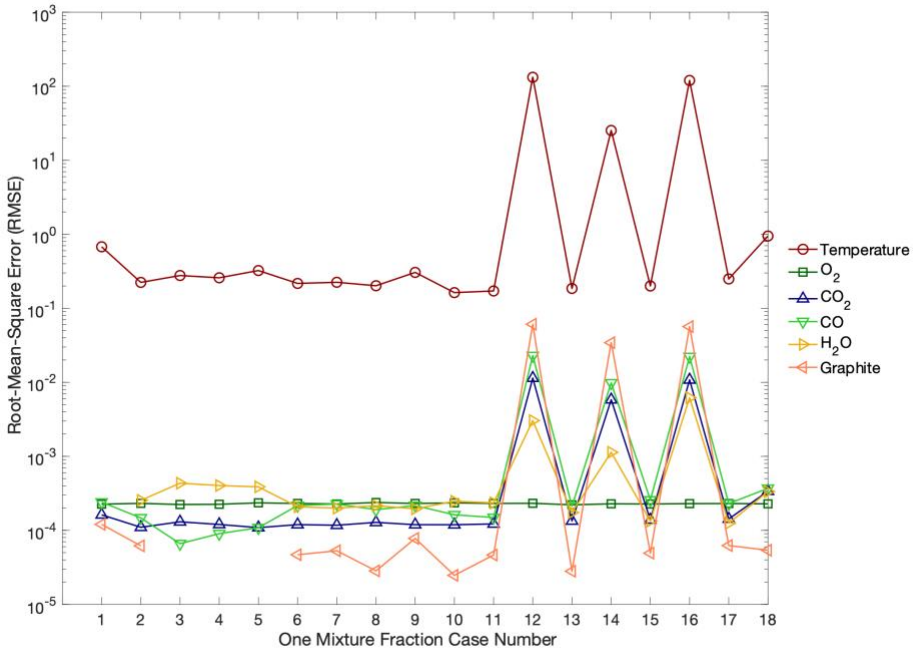

Figure 1. Root-mean-square error between NASA and Cantera Results

For the most part, there is good agreement between the NASA and Cantera results, however, a few of the highest rank coals (anthracites and semi-anthracites), the RMSE is quite high. From the statistical summary in Figure 1, it is unclear if those spikes in RMSE are a result

of the deviation of a single point or multiple points in the equivalence ratio range. Results from NASA and Cantera were plotted against each other for each fuel over the range of equivalence ratios to determine where the deviations occur. Figure 2 shows an example of good agreement between NASA and Cantera (Pitt 8 coal, case number 1-6) and poor agreement (Mammoth seam coal, case number 1-12) for equilibrium temperature and the mole fractions of H_2O and graphite. These parameters help to illustrate the reason for the deviation between NASA and Cantera and in which conditions the deviations occur. The lines are from NASA-CEA and the points are from Cantera. More detail on these equilibrium comparisons are found in Richards [70].

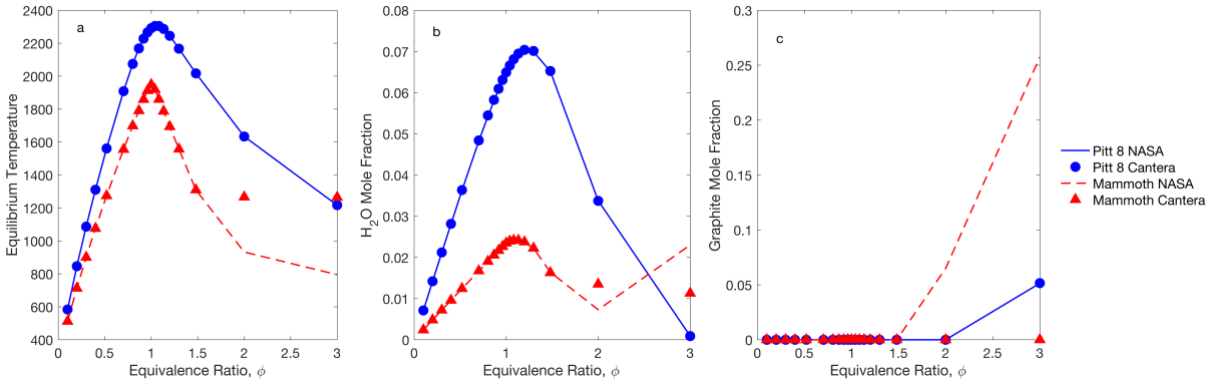

Figure 2. Comparison of NASA (lines) to Cantera (markers) results: (a) Temperature, (b) H_2O mole fraction, and (c) graphite mole fraction.

The statistical results shown in Figure 1 give an overall picture as to which fuels exhibit poor agreement. However, the poor agreement occurs only in fuel-rich conditions where $\phi >$ 1.5, as illustrated in Figure 2. NASA converts all unreacted fuel to graphite (indicated by the higher graphite mole fractions at higher equivalence ratios) whereas Cantera tends to leave some portion of the higher rank coals as unreacted fuel with the same composition and energy

properties. This is likely because of the way the Cantera equilibrium solver was set up to reduce numerical instabilities, which included separate mechanisms for the combustion gases, graphite, and the solid fuel. Because Cantera leaves some of the material as unreacted coal instead of converting it to graphite, the amount of graphite present at the highest equivalence ratios as well as the amounts of the other equilibrium products are decreased. The unreacted coal "species" contains higher amounts of hydrogen, oxygen, and other atoms than graphite. The disparity between NASA and Cantera only seems to occur with some higher rank coals. Most modern applications of coal combustion will fall outside of these extreme conditions when looking at the system as a whole, save for gasification or other specialized processes. However, there will likely be regions that are locally very fuel rich, especially in regions of coal pyrolysis where there are typically low concentrations of oxidizing gases close to the coal. Even with these few cases of deviation between NASA and Cantera, there is a low instance of disparity overall, which means Cantera can be used to adequately calculate the equilibrium states of multiple mixture fraction systems (with the exception of a few of the highest rank coals), which is more difficult to do with the stand-alone NASA code.

3.1.2 Full Fuel Comparison

The second question addressed by the one-mixture fraction comparison was to ascertain the difference is between coal types and various coal surrogate gases. Coal surrogate gases such as graphite, benzene, methane, ethylene and others have been used in the place of coal and coal-based fuels [39]. While these can be used in a combination to reach the correct atomic ratios, reaction and bond energies are harder to get correct, leading to inaccuracies in temperature and other important equilibrium factors. Surrogate gas enthalpies can be adequately matched to coal-

specific values by changing the surrogate gas temperature to obtain the correct enthalpy, however, this can result in gas temperatures that are outside the bounds of the curve fits for the polynomial thermodynamic models, leading to inaccurate thermodynamic property predictions. The surrogates used in this analysis do not have adjusted enthalpies but are instead used as a direct substitute for coal-based fuels.

To address these inaccuracies and to get an idea of how much error might be introduced into a large-scale simulation by using these simplifying assumptions, all fuel cases from Table 3 were directly compared against each other using equilibrium temperature and the mole fractions of O_2, CO_2, CO, H_2O, and graphite. Figure 3 shows the NASA results for equilibrium temperature, plotted using both the equivalence ratio and fuel mixture fraction. While this figure shows the results from the NASA code, the results from Cantera were virtually identical.

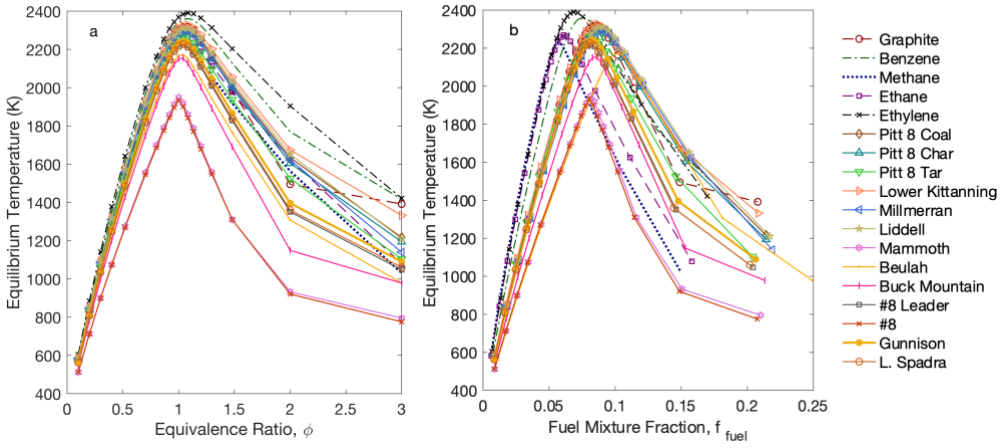

Figure 3. Equilibrium temperature calculations by the NASA-CEA code for all fuel cases: (a) vs. equivalence ratio and (b) vs. fuel mixture fraction.

Equilibrium temperature is strongly influenced by fuel type used, especially at or above stoichiometric mixtures. The peak temperature usually occurs at a mixture just fuel rich of the

stoichiometric point and the difference is around 400 to 500 K between the highest temperature fuel (ethylene) and the lowest temperature fuel (Mammoth seam anthracite). The temperature difference is even greater in the fuel-rich conditions ($\phi > 1$). For most fuels, the difference is minimal at very fuel lean conditions ($\phi \leq 0.5$), likely due to fuel being very dilute compared to the oxidizer. Using the fuel mixture fraction complicates the comparison slightly, shifting the peak temperatures to the left and right while keeping the peak temperature value the same. The comparison vs. equivalence ratio therefore makes more sense and will be used in the remainder of this paper. See Richards [70] for the remainder of the comparison vs. fuel mixture fraction.

The O_2 mole fraction comparisons did not show a lot of variability between fuels, and are not shown here (see Richards [70]). This lack of variability in equilibrium O_2 between the fuels is because most of the oxygen comes from the air with little to none from the fuel.

Figure 4 shows the CO_2 and CO mole fractions vs. equivalence ratio for the different fuels. There is wide variability in the equilibrium CO_2 mole fraction depending on which fuel is used, especially around stoichiometric conditions, which is where most industrial coal furnaces operate. Many of the coals fall in the middle range of the peak CO_2 mole fraction, with the coal surrogates lying toward both the top and bottom. The fraction of CO_2 would depend on the carbon content of the original fuel, with fuels enriched in carbon (high rank coals and graphite) generally having an increased CO_2 and CO content. The CO_2 content greatly influences the overall heat transfer properties of a coal boiler since CO_2 blocks a lot of radiative heat transfer in the gaseous environment. Generally, the ratio between CO_2 and CO are dependent on local gas temperature and local oxygen content.

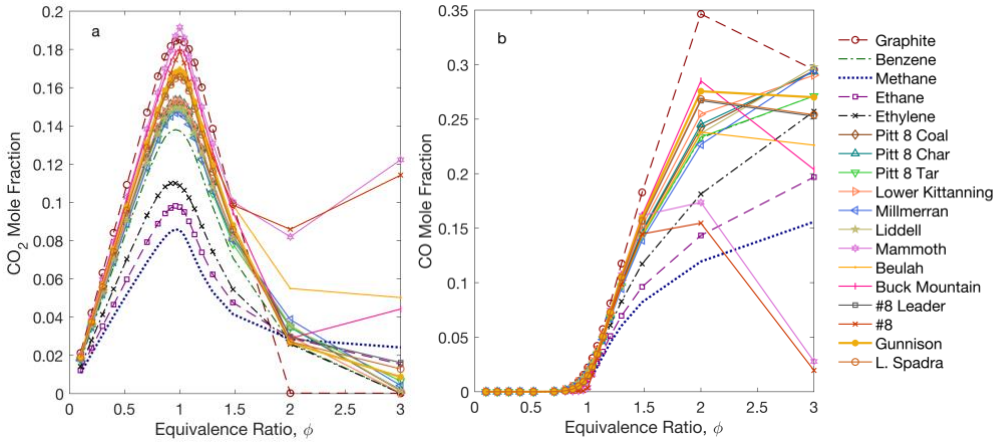

Figure 4. Equilibrium CO_2 and CO mole fraction calculations by the NASA-CEA code for all fuel cases: (a) CO_2 mole fraction vs. equivalence ratio and (b) CO mole fraction vs. equivalence ratio.

The CO mole fraction only becomes significant near stoichiometric conditions and moving into fuel rich conditions. This makes sense from a combustion perspective because there is less oxygen to completely oxidize the carbon in fuel rich conditions. The difference in calculated CO between fuels also increases at higher equivalence ratios. The decrease in CO (and increase in CO_2) at $\phi > 2$ is thought to be due to lower temperatures as well as the presence of graphite and unreacted fuel.

The H_2O and graphite mole fraction comparisons are shown in Figure 5. The H_2O mole fraction varies widely based on what fuel is used, from no H_2O with graphite to almost 20 mol% at the peak with methane. The amount will vary based solely on the amount of hydrogen in the original fuel since there is no additional hydrogen in the air. Also like the CO_2 mole fraction, the amount of water in a gaseous environment greatly influences the radiative heat transfer of the system. The equilibrium H_2O compositions for most coals again fall in the middle range of all fuels, with several surrogate gases lying to the extreme highs and lows of H_2O compositions.

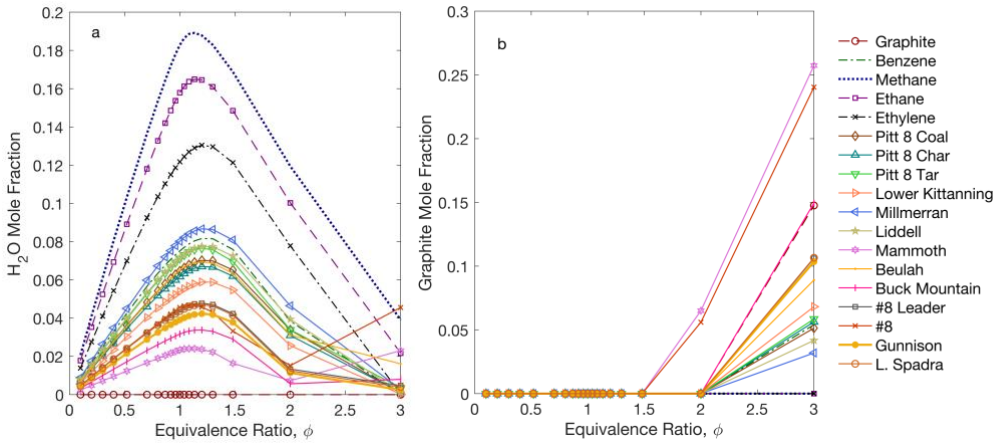

Figure 5. Equilibrium H_2O and graphite mole fraction calculations by the NASA-CEA code for all fuel cases: (a) H_2O mole fraction vs. equivalence ratio and (b) graphite mole fraction vs. equivalence ratio.

Graphite only shows up in the most fuel rich conditions, acting as a surrogate for "unreacted" fuel, char, and soot, with most fuel cases only showing graphite formation at equivalence ratios of 2 and higher. Unreacted fuel is almost always a problem if it is present at the end of combustion, especially when attempting to obtain the maximum amount of energy from a fuel.

Using simple hydrocarbons as surrogate gases for coal and coal-based fuels (char, tar, light gases, etc.) makes equilibrium calculations simpler and faster. However, using these surrogates as a direct replacement for coal-based fuels introduces a large amount of variability, especially at higher equivalence ratios (extreme fuel-rich conditions). This is particularly the case for CO_2 and H_2O content, and to a lesser degree equilibrium temperature and CO content. The majority of the inconsistencies between real coal values and surrogate gases could perhaps be mitigated to a degree by dialing in the enthalpy of the surrogates by changing the reference

579 temperature at which the enthalpy is calculated, however, this could potentially lead to
580 improbable or even impossible temperatures. For these reasons, it is much better to use the actual
581 physical and chemical properties of the coal (when available) instead of simplifying it with a
582 surrogate gas.
583
584 3.2 Two Mixture Fractions
585 The two-mixture fraction comparison breaks the fuel stream into two separate streams,
586 one for mass originating in the char and one for the volatiles. Like the one-mixture fraction
587 comparison, there are two main questions addressed by the two-mixture fraction comparison: (1)
588 how close are the results using the reported tar properties rather than full volatiles (by combining
589 tar and light gas properties) and (2) can char and volatile surrogate gases be used in the place of
590 real char and volatiles properties? The first question is raised because some pyrolysis
591 experiments report only tar yields, compositions, and heating values but not light gas properties
592 with which to calculate values for the total volatiles. Table 4 shows the fuel cases tested in the
593 two-mixture fraction comparison. Note that Cantera was the only equilibrium program used in
594 this comparison as a matter of convenience.
595
596 Table 4. Two-Mixture Fraction Fuel Cases

Case Number	Char	Volatiles	Reported Volatiles Yield
2-1	Graphite	Benzene	
2-2	Graphite	Methane	
2-3	Graphite	Ethane	

2-4	Graphite	Ethylene	
2-5	Pitt 8 Char (Low Temperature)	Pitt 8 TAR (Low Temperature)	0.1491
2-6	Pitt 8 Char (High Temperature)	Pitt 8 TAR (Low Temperature)	0.4102
2-7	Pitt 8 Char (Low Temperature)	Pitt 8 VOLATILES (Low Temperature)	0.1491
2-8	Pitt 8 Char (High Temperature)	Pitt 8 VOLATILES (High Temperature)	0.4102
2-9	Millmerran Char (High Temperature)	Millmerran TAR (High Temperature)	0.545
2-10	Millmerran Char (High Temperature)	Millmerran VOLATILES (High Temperature	0.545
2-11	Millmerran Char (Low Temperature)	Millmerran TAR (Low Temperature)	0.313
2-12	Millmerran Char (Low Temperature)	Millmerran VOLATILES (Low Temperature)	0.313

597

598 To get the whole range of fuel mixing conditions, equilibrium states for each case were
599 calculated in the equivalence ratio range of 0.1 to 3 for each of 5 or 6 fuel mixing conditions
600 ranging from no volatiles to all volatiles (Y_{vol} = 0, 25, 50, 75, and 100% of the fuel, and the
601 reported volatiles yield for each of the coals, which is an intermediate percentage between 10 and
602 60% of the DAF coal depending on pyrolysis conditions and coal type). The same variables of

603 interest used in the one-mixture fraction comparison (temperature and the mole fractions of O_2,
604 CO_2, CO, H_2O, and graphite) were compared for all cases listed in Table 4. To illustrate the
605 temperature profiles for each fuel mixing condition, Figure 6 shows contour plots of the
606 equilibrium temperature for two fuel cases (2-1, graphite and 2-8, Pitt 8 coal) for all fuel mixing
607 conditions. The columns represent the percent of the fuel that was volatiles (vs. char) and the
608 rows represent the given fuel considered.
609

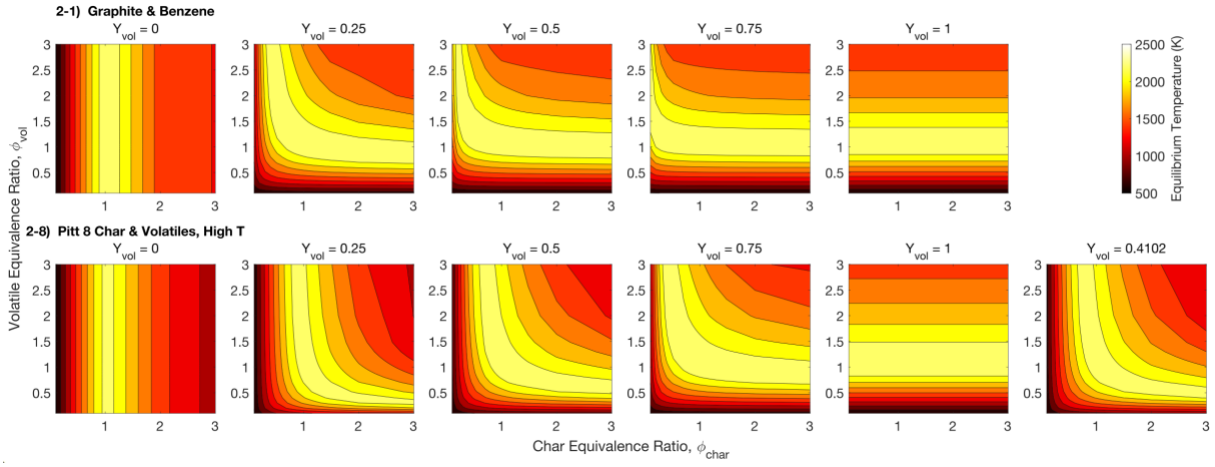

610

611 Figure 6. Equilibrium temperature calculations by Cantera. Note that all plots have the same
612 color range, as shown in the color bar in the upper right corner of the plot.
613

614 Only two cases were used here to demonstrate the trends between cases and fuel mixing
615 ratios. The plots for the other cases listed in Table 4 are found in Richards [70]. A given column
616 in Fig. 6 shows a given fuel mixing condition for each type of fuel. The general shapes are
617 similar, however, there are slight differences, especially with a higher volatiles mixture (Y_{vol} ≥
618 75%). The difference in shape of the temperature curves is more pronounced between the coal-
619 based fuels and the simpler surrogate gas fuels (not shown) but is less pronounced among the
620 coal-based fuels, which is similar to the trends observed in the one-mixture fraction comparison.

In addition, the simpler fuels tend to have higher temperatures than the coal-based fuels, particularly around stoichiometric conditions. Figure 7 shows the peak temperature ranges of all fuel cases listed in Table 4. The circles for each case represent the peak equilibrium temperature for each value of Y_{vol}. For example, the peak temperatures in each of the subplots in Fig. 6 for Case 2-8 range from 2250 K for $Y_{vol} = 0$ to almost 2400 K for $Y_{vol} = 1$. These temperature differences, even small differences, can potentially impact the accuracy of large-scale simulations, especially in fuel-rich conditions where the difference is more pronounced.

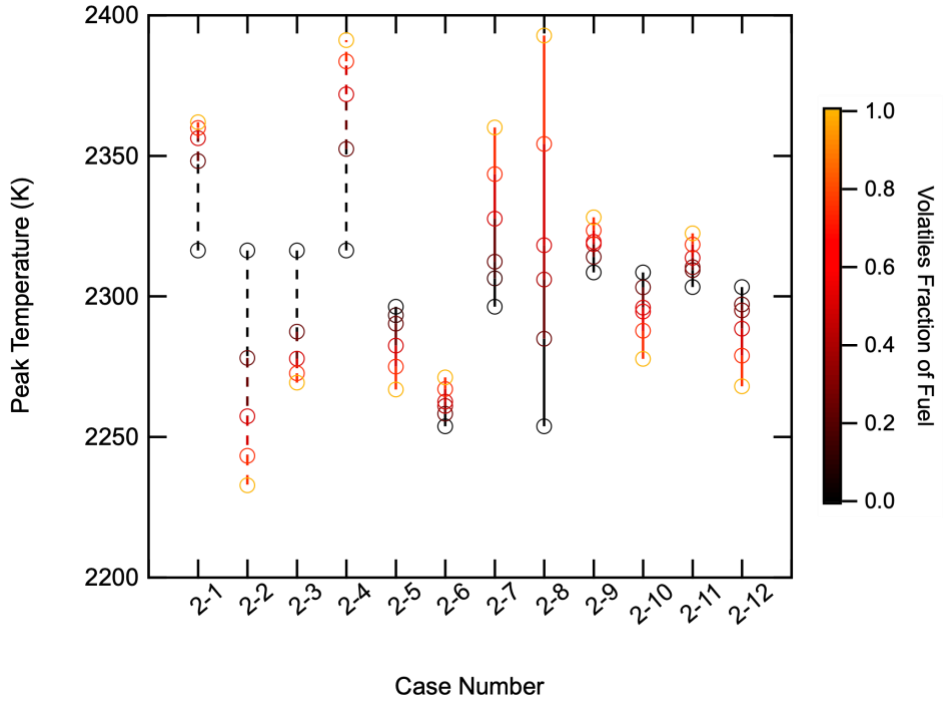

Figure 7. Peak temperature range for all fuel cases. Dashed lines correspond to simple surrogate gases and the circles correspond to each fuel mixing condition. The color of the lines and dots depends on the fuel mixing ratio (Y_{vol} ranging from 0 to 100% volatiles).

The first part of this analysis was to determine if measured tar properties could reasonably be used as a surrogate for the total volatiles. There were four comparisons between tar and total volatiles: 1) cases 2-5 and 2-7, 2) cases 2-6 and 2-8, 3) cases 2-9 and 2-10, and 4) cases 2-11 and 2-12. Figure 7 shows that there is enough variability between the tar and volatiles cases that it is not a good idea to use tar instead of total volatiles. For example, the temperature range for case 2-6 spans less than 50 K while that for case 2-8 spans almost 150 K. Most of the similarity in the calculated temperatures comes from the char-only fuel mixtures (black circles, where $Y_{vol} = 0$). The extremes of char-only (black circles) and volatiles-only (yellow circles, $Y_{vol} = 1$) fuel mixtures would fall directly in line with the one-mixture fraction results using char-only or volatiles-only fuels. The one-mixture fraction results using the original coal properties of fuel would likely be better compared to the two-mixture fraction results where the char and volatiles are more evenly split (close to a Y_{vol} of 0.5) or the pyrolysis yield results (e.g., Y_{vol} of 0.4102).

The peak temperature depends highly on the fuels used in the two-mixture fraction system. Some mixtures have larger ranges (2-8, which uses the measured properties of high temperature Pitt 8 pyrolysis products), while many others have much smaller ranges. Some of the surrogate gas cases are encompassed by the measured coal-based fuel cases, but others have no overlap. There is a large variability in the range and limits of equilibrium temperature depending highly on the fuels used. While these are peak adiabatic temperatures, which occur near $\phi_{tot} = 1$, the discrepancies due to the fuel assumption would likely be very similar when used in real, non-adiabatic systems.

The mole fractions of the key combustion-related species at equilibrium were also compared in graphs like Figs. 6 and 7. Like the one-mixture fraction comparison, the O_2 mole fraction does not differ much between fuel cases, so the contour plots are not shown here, but

657 can instead be found in Richards [70]. Because of the similarity of the equilibrium O_2 mole
658 fractions between fuels, the shapes and ranges are all very similar. This is understandable
659 because the majority of the oxygen content comes from the air, even with coal-based fuels that
660 have oxygen bound in the organic matrix. The peak O_2 mole fractions for each fuel case and fuel
661 mixing condition are shown in Figure 8.
662

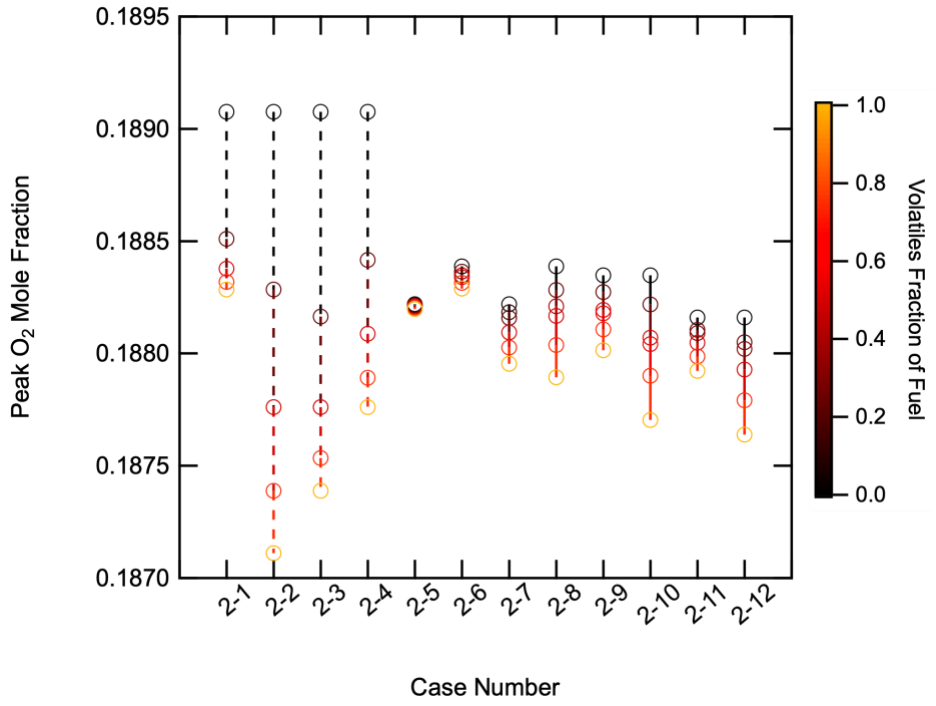

663
664 Figure 8. Peak O_2 mole fraction range for all fuel cases. Dashed lines correspond to simple
665 surrogate gases and the circles correspond to each fuel mixing condition. The color of the lines
666 and dots depends on the fuel mixing ratio (Y_{vol} ranging from 0 to 100% volatiles).
667
668 While Figure 8 seems to show a large variability in oxygen mole fraction, especially in
669 the ranges between the simple coal gas surrogates (first four lines from the left) and the coal-
670 based fuels, the axis range makes it seem larger. The peak O_2 mole fraction only ranges between

0.187 and 0.189. In addition, these peak O_2 mole fractions only occur at the lowest equivalence ratios, in extreme fuel-lean conditions. This shows that the equilibrium oxygen content is not highly dependent on the fuel used in equilibrium calculations, but more dependent on the fuel-to-oxidizer ratio used in the combustion process.

In the one-mixture fraction comparison, the CO_2 mole fraction varied highly depending on the fuel type used. A representative CO_2 mole fraction comparison of contour plots for the two-mixture fraction calculations are shown in Figure 9 (a complete series of plots are given in Richards [70]).

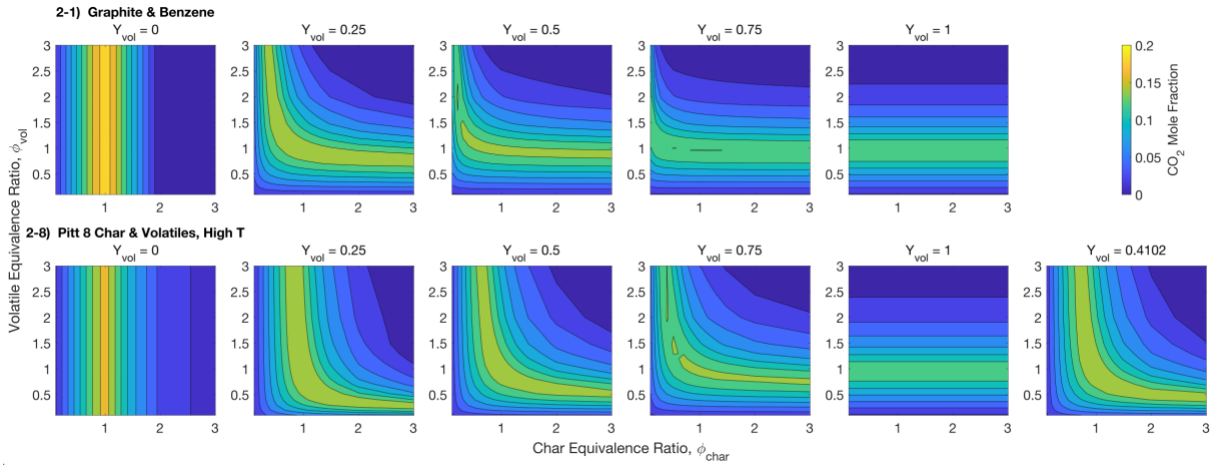

Figure 9. Equilibrium CO_2 mole fraction calculations by Cantera. Note that all plots have the same color range, as shown in the color bar in the upper right corner of the plot.

Like the one-mixture fraction comparison, CO_2 follows the same general trend as the temperature curves. However, like the temperature curves, the range of peak CO_2 mole fractions are very different for each fuel. There are major differences when comparing the coal-based mixtures to the coal surrogate gas mixtures. The four surrogate gas mixtures approximate the char as pure carbon (graphite) and the volatiles surrogate changes with each case. With more

char (graphite), the CO_2 fraction is much greater than for the coal-based mixtures at the same fuel mixing conditions, whereas when the volatiles are more favored in the mixture, the CO_2 mole fraction is a lot lower than the coal-based mixtures. This is because of the large discrepancy in the carbon content of the coals and coal surrogate gases. Graphite is pure carbon (much higher in carbon than any of the coal-based fuels) and the other simple hydrocarbon fuels have a lower carbon fraction than the coal-based fuels. The ranges of peak CO_2 mole fractions for each fuel case are shown in Figure 10.

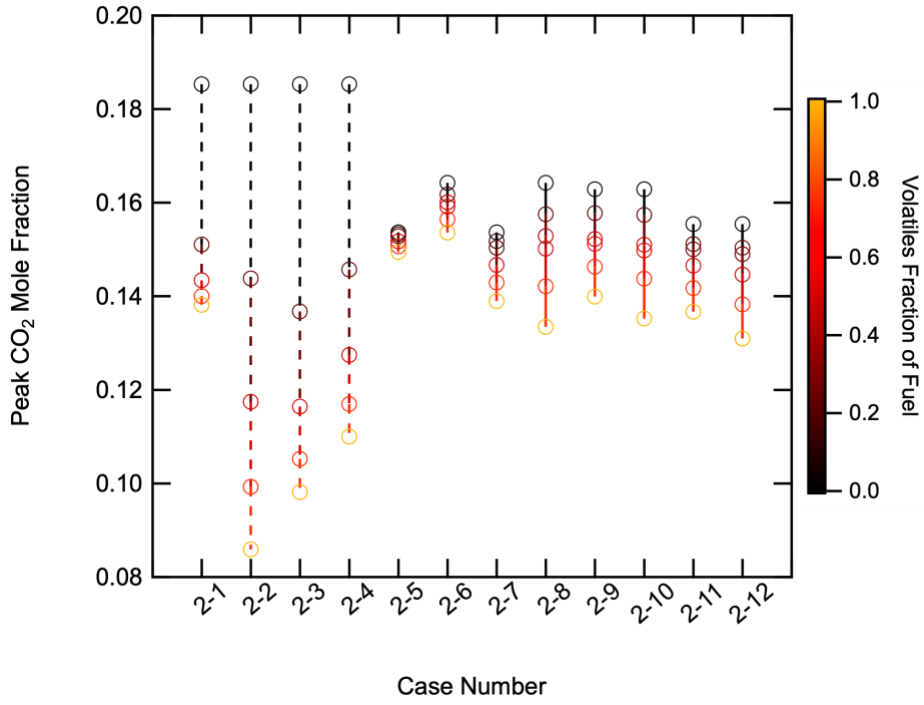

Figure 10. Peak CO_2 mole fraction range for all fuel cases. Dashed lines correspond to simple surrogate gases and the circles correspond to each fuel mixing condition. The color of the lines and dots depends on the fuel mixing ratio (Y_{vol} ranging from 0 to 100% volatiles).

The CO_2 mole fraction increases when more oxygen is present for complete combustion to occur. However, the peak CO_2 mole fraction differs from the O_2 mole fraction in the overall range of values. The peak CO_2 range is largest with the coal surrogate gases and smaller in the coal-based fuels, with a maximum range between 8 and 19%. Note that the coal-based fuels include some fuel-bound oxygen while the surrogates contain no additional oxygen.

The ratio between the CO_2 and CO mole fractions is dependent on both local temperature and O_2 content. Because of this, the CO/CO_2 ratio increases as ϕ increases until graphite starts to form. The CO mole fraction contours for cases 2-1 and 2-8 are shown in Figure 11.

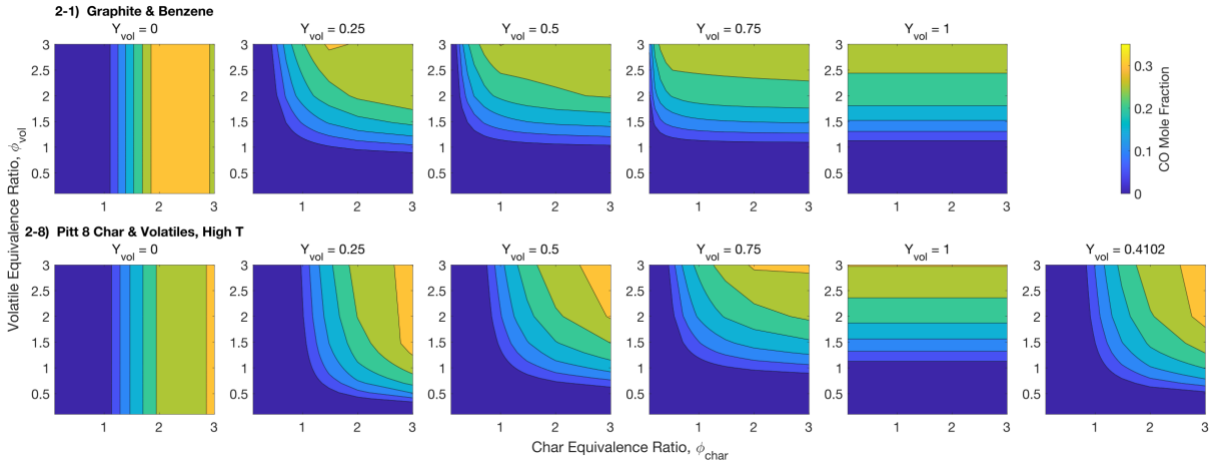

Figure 11. Equilibrium CO mole fraction calculations by Cantera. Note that all plots have the same color range, as shown in the color bar in the upper right corner of the plot.

Because of the lower oxygen content, CO becomes more prevalent in fuel rich conditions. There is very little difference in the shape of these contours between the CO mole fraction from tar properties compared to the CO mole fraction of total volatiles properties. Like the CO_2 mole fractions, the differences become slightly more pronounced with higher volatiles mixtures, particularly in the gradient, or how fast CO increases with increasing equivalence ratio.

720 There is a significant difference between the calculated CO of the coal-based fuels and
721 the simplified surrogate gases, as seen for the CO_2 mole fractions. In mixtures that are almost all
722 graphite, there is a larger range of very high CO mole fractions. However, with mostly volatile
723 surrogates, the CO mole fraction is much smaller than with coal-based fuels. The peak CO mole
724 fraction ranges for each fuel case are shown in Figure 12.
725

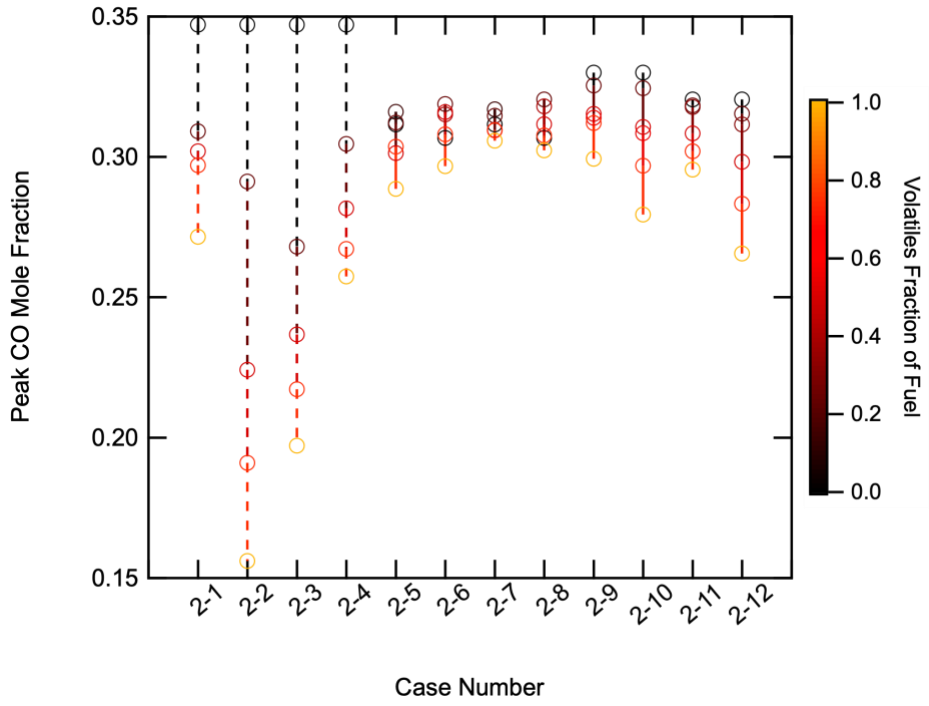

726
727 Figure 12. Peak CO mole fraction ranges for all fuel cases listed in Table 4. Dashed lines
728 correspond to simple surrogate gases and the circles correspond to each fuel mixing condition.
729 The color of the lines and dots depends on the fuel mixing ratio (Y_{vol} ranging from 0 to 100%
730 volatiles).
731
732 The peak CO mole fraction ranges follow a very similar trend as the CO_2 mole fractions,
733 although with even greater ranges, from 15 to 35 mol%. The peak CO mole fractions, however,

occur only in extreme fuel-rich conditions. This trade-off between the locations of greatest CO and CO_2 mole fractions is because the ratio of carbon dioxide and carbon monoxide are based on the available oxygen and temperature of the gas environment.

In the one-mixture fraction comparison, the H_2O mole fraction was very different depending on what fuel was used in the equilibrium calculations. The H_2O mole fraction contours for the two-mixture fraction comparison are given in Figure 13.

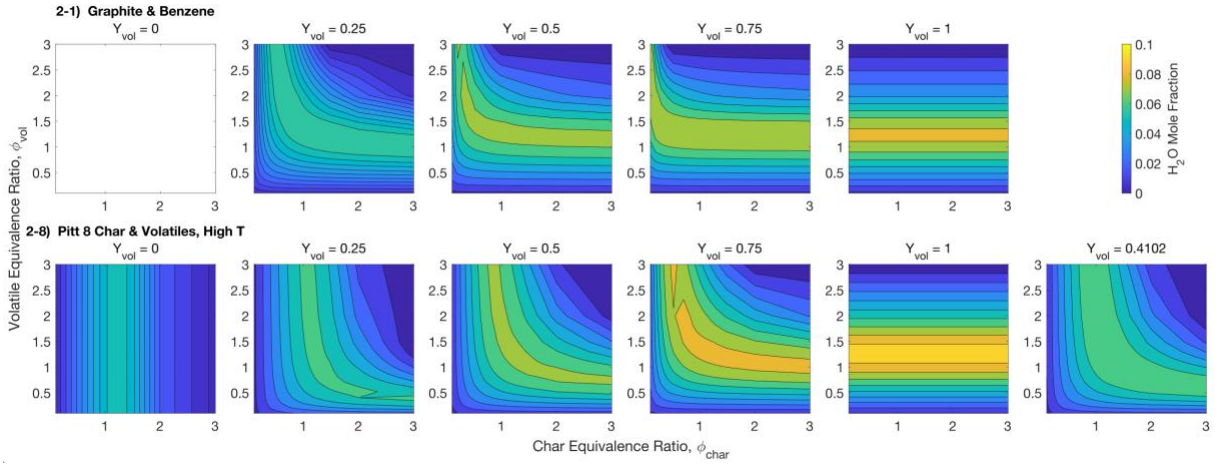

Figure 13. Equilibrium H_2O mole fractions as calculated by Cantera. Note that the plots for pure graphite show as a blank plot (top left) because graphite has no hydrogen to form H_2O.

There is a significant difference in the H_2O mole fraction when using tar properties compared to total volatiles, and an even greater difference when using surrogate gases. It is worth noting in the "char only" (first column) mixtures of the surrogate fuels, the plots appear to be blank. This is not a mistake, rather, the fuel mixture is entirely graphite in those equilibrium states, and therefore there is no fuel hydrogen to contribute to an equilibrium moisture content. There is no additional hydrogen in the air, so the H_2O mole fraction at equilibrium is entirely dependent on the hydrogen content of the original fuel. In addition, the moisture content of the

equilibrated mixture highly influences both gasification reactions and radiative heat transfer in the combustion system.

The peak H_2O mole fraction ranges are shown in Figure 14. The peak H_2O mole fraction is highly dependent on the fuel chosen (similar to the one-mixture fraction results) and can range from no H_2O produced (graphite) to almost 20 mol% produced (methane). Fuels with a higher hydrogen fraction end up with a higher equilibrium moisture content than fuels with less hydrogen. In coal pyrolysis, the volatiles tend to become enriched in hydrogen, especially in the light gas species that include compounds like methane (CH_4), ethane (C_2H_6), ethylene (C_2H_4) and other simple hydrocarbons. Accurately determining where fuel hydrogen is and when it is accessible to gas-phase chemistry is very important in determining other heterogeneous reactions as well as radiative heat transfer. This is not as important with a one-mixture fraction system but becomes more important in two- or three-mixture fraction systems.

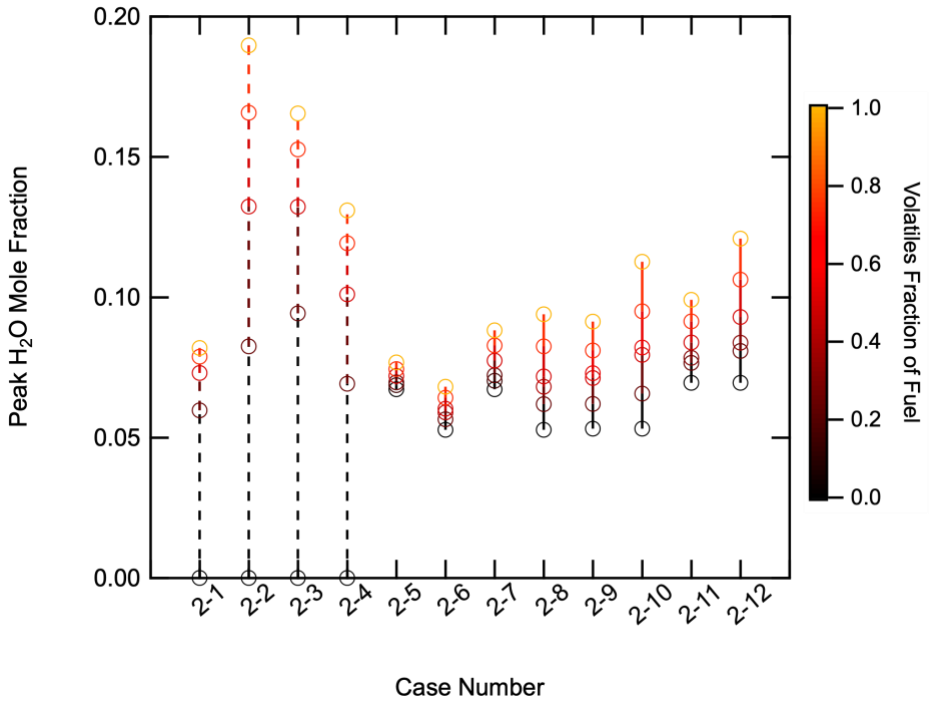

Figure 14. Peak H_2O mole fraction ranges for all two-mixture fraction fuel cases listed in Table 4. Dashed lines correspond to simple surrogate gases and the circles correspond to each fuel mixing condition. The color of the lines and dots depends on the fuel mixing ratio (Y_{vol} ranging from 0 to 100% volatiles).

Graphite (solid carbon) was shown in the one-mixture fraction approach to only matter in fuel-rich conditions. Industrial combustion applications usually do not operate in such conditions because it usually means some of the original fuel is not being completely burned, which can greatly impact many aspects of a combustion apparatus. The graphite mole fraction contours for cases 2-1 and 2-8 are shown in Figure 15.

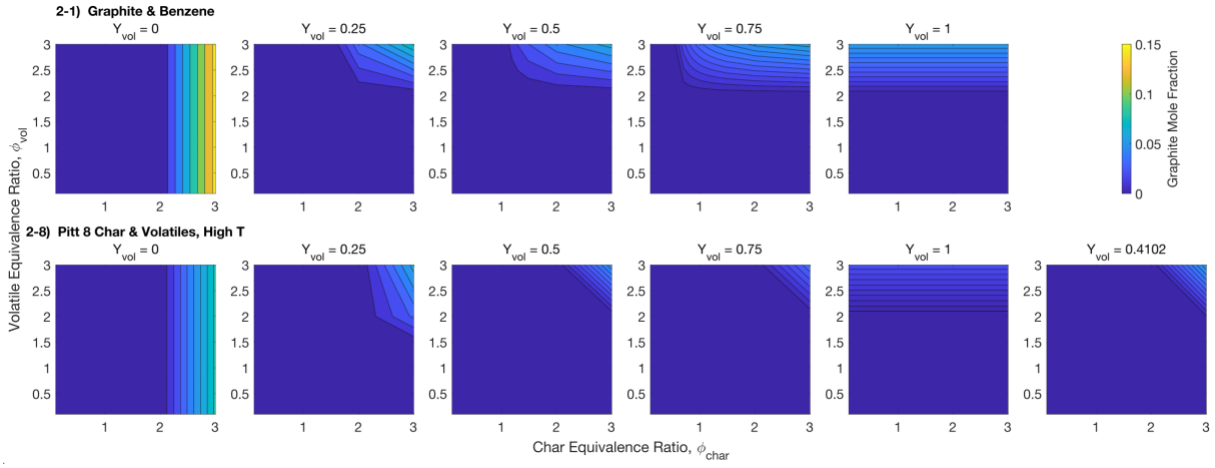

Figure 15. Equilibrium graphite mole fractions as calculated by Cantera. Note that all plots have the same color range, as shown in the color bar in the upper right corner of the plot.

Like the one-mixture fraction comparison, many of the fuel mixtures in the two-mixture fraction comparison have very little graphite formation and only in the extreme fuel-rich

783 locations. The peak graphite mole fraction ranges for each two-mixture fraction case are shown
784 in Figure 16.
785

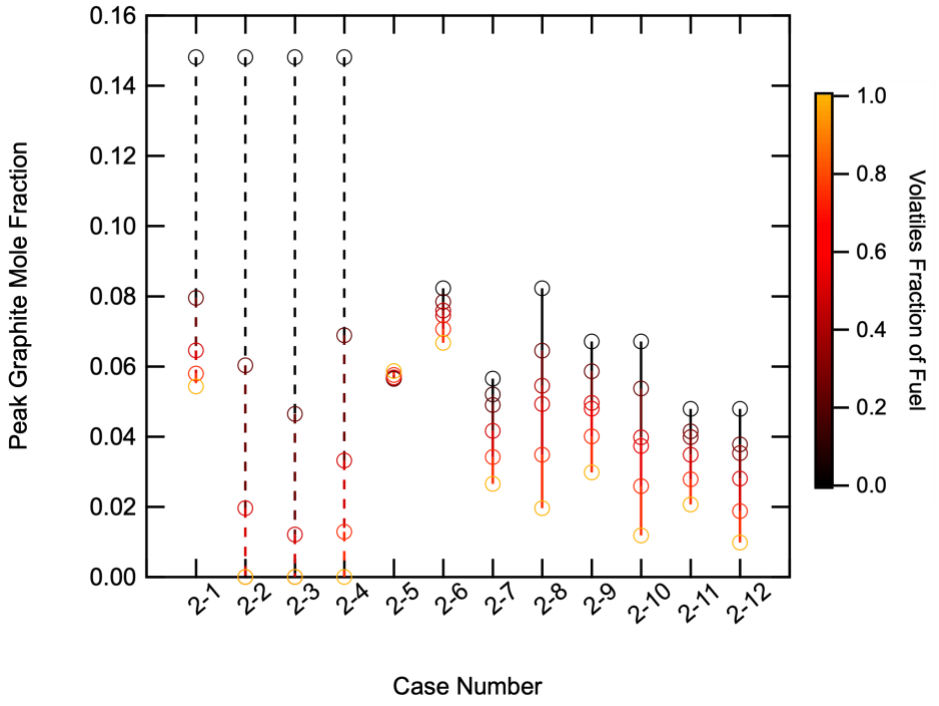

786

787 Figure 16. Peak graphite mole fraction ranges for all two-mixture fraction fuel cases listed in
788 Table 4. Dashed lines correspond to simple surrogate gases and the circles correspond to each
789 fuel mixing condition. The color of the lines and dots depends on the fuel mixing ratio (Y_{vol}
790 ranging from 0 to 100% volatiles).
791

792 The ranges of peak graphite mole fractions are quite varied, with the largest ranges in the
793 surrogate gases, ranging between no equilibrium graphite to 15 mol% in the pure graphite fuel
794 mixtures. None of the coal-based fuels exceed 9 mol% graphite at equilibrium, and many of the
795 fuel cases fall well below that percentage. Incorrectly calculating solid carbon at equilibrium

could cause major errors in large-scale simulations, particularly in deciding how much over-fire air might be needed to completely burn out the original fuel.

A two-mixture fraction approach seems to be more appropriate for coal-based fuels than a one-mixture fraction approach. In an industrial coal boiler, the coal particles enter the hot environment (typically in slightly fuel rich conditions) and almost immediately begin to pyrolyze. The whole pyrolysis process typically lasts milliseconds with the high particle heating rates of pulverized coal particles. This means that the local gas composition is a mix of oxidizer and volatile gases from the coal. The char remains a solid until the reactive gases can make it to the char surface and begin to react, adding mass from the char into the gas mixture. This means that coal pyrolysis and char conversion can be easily described using separate mixture fractions. Care must be taken when choosing the compositions and heating values of the volatiles and char. The results here indicate that choosing a simple volatile or char surrogate gas as a direct replacement for measured coal properties results in large differences in the equilibrium mole fractions of CO_2, CO, and H_2O. Much of this difference in equilibrium composition can be traced back to the difference in elemental compositions between fuels, as illustrated in Table 2. This is one of the key reasons why more than one mixture fraction is needed to accurately describe coal combustion reactions.

3.3 Three Mixture Fractions

Because coal pyrolysis results in three main products (char, tar, and light gas), coal pyrolysis can be easily divided into a three-mixture fraction approach. There was only one coal that included enough information to calculate an average light gas composition and heating value—the Pitt 8 coal, specifically with low temperature pyrolysis products (char, tar, and light

gases). Because only one fuel was used to calculate equilibrium states based on a three-mixture fraction system, the results for this fuel were compared against the results for the same fuel using both one and two mixture fractions.

The procedure used to set up the three-mixture fraction comparison is described in greater detail in the introduction and approach sections; however, it is similar to the approach used in the two-mixture fraction comparisons, with the fuel mixing conditions being slightly more complex. In this case, the fractions of char and tar were allowed to vary between 0 and 1, including the fractions of each at the reported pyrolysis conditions. The fraction of light gas was the remainder of the fuel mixture, and the sum of the three fuel fractions was constrained to sum to one. The oxidizer was handled the same way here as in the one- and two-mixture fraction approaches. The oxidizer contribution for each fuel stream was allowed to vary independently in an equivalence ratio between 0.1 and 3, with all stream contributions weighted by the fractions of each fuel stream.

The one-mixture fraction approach calculated at about 20 different equilibrium states over the whole range of equivalence ratios for each fuel; the two-mixture fraction approach calculated around 2,000 equilibrium states for each fuel; and the three-mixture fraction approach calculated almost 150,000 equilibrium states for a single fuel. The one-mixture fraction approach finished in generally under a minute for each fuel; the two-mixture fraction approach took anywhere from an hour to a couple of days in Cantera; and the three-mixture fraction approach took four or more days on a single processor.

Because of the large amount of data generated in the three-mixture fraction comparison, it would be difficult to compare the results of the coal-based fuels to the simple surrogate gases in any meaningful way. A more meaningful approach compares the results of all three mixture

fraction approaches for one fuel. The same key variables were used to compare all three mixture fractions together, starting with the equilibrium temperature and H_2O mole fraction shown in Figure 17. To compare similar values, all of these comparison plots are made with respect to the carbon mixture fraction (Z_c) rather than any of the component mixture fractions (f_i) or equivalence ratios. For comparisons using the same parent fuel, any individual elemental mixture fraction, Z_j, would have the same range regardless of the number of component mixture fractions used, while allowing for a comparison of all mixture fraction approaches on one figure in one mixture fraction dimension. In this comparison, the carbon mixture fraction seemed to be the most appropriate to use since the bulk of the fuel is comprised of carbon.

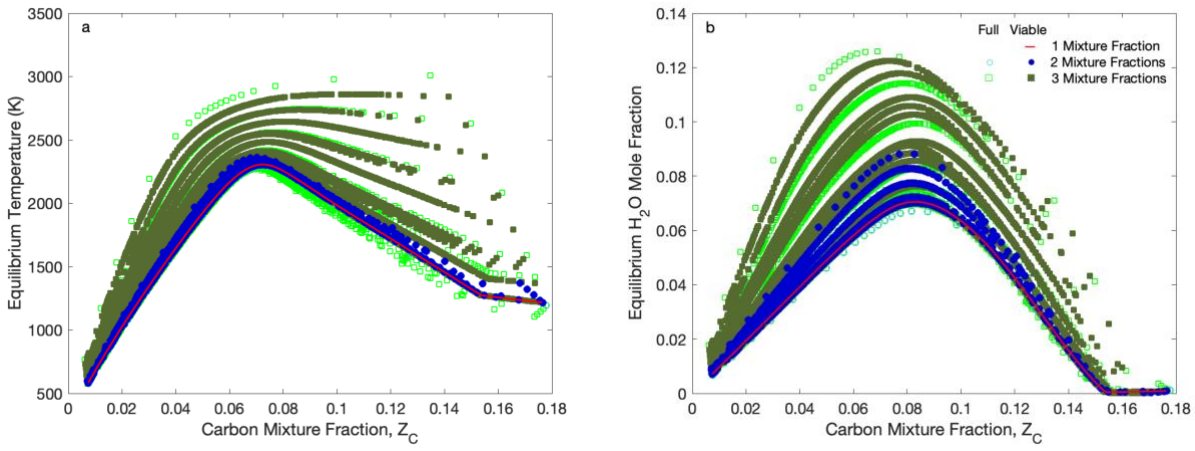

Figure 17. (a) Equilibrium temperature and (b) H_2O mole fraction calculations by Cantera for the Pitt 8 coal using one (case 1-6), two (case 2-7), and three mixture fractions. Note that the two- and three-mixture fraction results are shown as "viable" and "full." The viable results only including results for mixtures of fuels with the maximum char yield based on pyrolysis measurements.

Two sets of results are displayed for both the two- and three-mixture fraction approaches. The "full" results include all equilibrium states over the full range of fuel mixing conditions and the "viable" results limit the fuel mixing conditions to have a maximum char yield based on pyrolysis measurements. In combustion applications, the other pyrolysis products (tar and light gas) enter the gas phase before the solid char begins to react with the gas phase. For this reason, there are situations where there might be equilibrium between the volatile gases (tar and light gases) before any material from the char mixes in with the gas phase, but the reverse situation (i.e., all char and no pyrolysis gases) would not occur unless the starting fuel was only char.

The peak temperature changes with the fuel mixing condition, especially in the three-mixture fraction approach. Each distinct "line" of data points in the three-mixture fraction results corresponds to a different fuel mixing condition (i.e., a different set of f_i's). The temperatures for the one- and two-mixture fraction approaches (Figure 17a) are very close to each other, with the two-mixture fraction temperatures having a slightly increased range (shown here as a wider temperature band). The three-mixture fraction approach, however, allows for much hotter temperatures (up to almost 3,000 K) in addition to some fuel mixtures with similar temperatures to both the one- and two-mixture fraction approaches. The hotter temperatures achieved by the three-mixture fraction approach correspond to mixtures with greater percentages of the light gas species, which would include some of the same simple hydrocarbon surrogates with much higher temperatures shown in the one-mixture fraction comparison. Both the two- and three-mixture fraction results include many more equilibrium states than the one-mixture fraction results.

In the one- and two-mixture fraction approaches, the H_2O mole fraction was highly dependent on the fuel used. This result was also seen in the three-mixture fraction approach (see Richards [70]), although the only case shown in Figure 17 is for a coal with realistic

882 compositions and heating values of char, tar, and light gas. Note that this set of data was from a
883 low temperature pyrolysis experiment. The H_2O mole fraction is highly dependent on the fuel
884 mixing conditions (how much of char, tar, and light gases are mixed into the overall reactant
885 mix). The peak H_2O mole fraction in Figure 17 varies between 6 and 13 mol% for the three-
886 mixture fraction approach and between 6 and 8 mol% using two mixture fractions. This large
887 variability might be enough to cause large errors in large-scale simulations if fewer mixture
888 fractions or even simple coal surrogate gases are used in the place of more complex mixture
889 fraction approaches.

890 Moisture can play a large role in large-scale combustion simulations, contributing to
891 additional chemical reactions (mainly gasification) and impacting radiative heat transfer
892 calculations. This was discussed to some extent in the two-mixture fraction comparison,
893 however, in a three-mixture fraction system, knowing where hydrogen is in a system is even
894 more important. The light gas components tend to be much more enriched in hydrogen than
895 either the char or the tar. This is one of the reasons for the large variability in the equilibrium
896 H_2O mole fraction in a three-mixture fraction system as opposed to a one- or two-mixture
897 fraction system.

898 The equilibrium O_2 mole fraction was very similar over all fuel mixing conditions even in
899 the three-mixture fraction calculations, and are not shown here (see Richards [70]). The CO_2
900 mole fraction had a wide range in both the one- and two-mixture fraction comparisons,
901 depending on the fuel choice. Figure 18 shows the comparison of the one-, two-, and three-
902 mixture fraction calculations of the mole fractions of CO_2 and CO for the Pitt 8 coal. The carbon
903 in the fuel is the only source of carbon in these equilibrium calculations, so small changes in the
904 total amount of each fuel component greatly influence the overall amount of CO_2 formed at

equilibrium. Including light gases as a separate fuel stream changes the amount of CO_2 even more since the carbon content is greatly reduced in light gas components that tend to be enriched in hydrogen (e.g., methane) or oxygen (like CO or CO_2). The three-mixture fraction calculations show that CO becomes more prominent in fuel-rich conditions where the carbon cannot fully oxidize to CO_2. This result is similar to the findings from the one- and two-mixture fraction calculations. However, the CO mole fraction also tends to be a little more spread out in the three-mixture fraction approach for Z_c values ranging from 0.04 to 0.09.

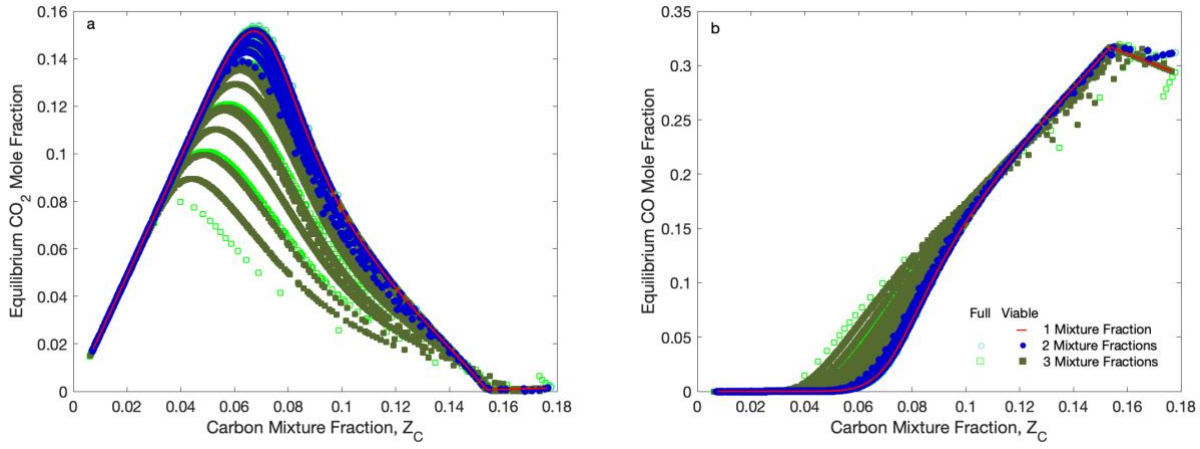

Figure 18. (a) Equilibrium CO_2 and (b) CO mole fraction calculations by Cantera for the Pitt 8 coal using one, two, and three mixture fractions.

In summary, the three-mixture fraction approach results in much more variety in equilibrium states than a simpler one- or two-mixture fraction approach, which would likely increase overall accuracy of coal combustor simulations using gas-phase equilibrium calculations. However, this greater variety would of necessity include significantly greater computational time and complexity. A two-mixture fraction approach that combines the tar and

light gases into a single “volatiles” mixture fraction would give greater variability and accuracy than a single coal mixture fraction while not greatly increasing computational complexity.

3.4 Implications for Large Simulations

Carbon dioxide and water are two gases that greatly impact radiative heat transfer. Both of these gases are highly influenced by both the original fuel used and the number of mixture fractions used. The equilibrium H_2O mole fraction in particular varies widely from zero with pure graphite in the one- and two-mixture fraction approaches to almost 20 mol% when using only methane as a surrogate gas in place of coal. Even when using measured values from coal and coal-based fuels there is a moderate amount of variability in both CO_2 and H_2O mole fractions, regardless of the number of mixture fractions used.

While a three-mixture fraction approach increases the variability of equilibrium states, it also greatly increases the computational time and complexity, often more than is desirable for large-scale simulations. In large-scale simulations, equilibrium calculations are often used to generate lookup tables to use in calculating the gas chemistry reactions, which means most of the time spent on equilibrium calculations would be incurred at the beginning of a simulation. When parallelized, the equilibrium calculations likely would not be significant compared to the overall simulation time, potentially only being an issue in smaller simulations. A two-mixture fraction approach that splits coal fuels into char and total volatiles can strike a better compromise between increased variability and accuracy while keeping the computational complexity low. In industrial applications, pyrolysis often occurs so fast that it is hard to distinguish a difference in when tars and light gases enter the gas phase.

One of the conclusions from Flores and Fletcher [50] was that their two-mixture fraction approach would be better than a one-mixture fraction analysis in accurately accounting for soot precursors. Tar was modeled as a constant fraction of the volatiles. In coal combustion systems, the primary source of soot precursors is the tar [71, 72]. A two-mixture fraction approach would be much better than a one-mixture fraction approach for modeling tar precursors, but a three-mixture fraction approach that models tar separately from light gases would seem to be most beneficial in calculating soot precursors. Hybrid approaches have been used where a mixture fraction of tar is solved for soot formation purposes but not fully integrated into the gas-phase chemistry calculations [71, 72].

The use of two or three fuel mixture fractions would not affect the outlet equilibrium composition of a combustor or gasifier if the coal achieved 100% conversion. The region of the combustor that would be most affected would be near the burner after pyrolysis but before significant char combustion or gasification occurred. This near-burner region plays a significant role in the formation of pollutants such as NO_x and soot, and therefore accurate calculations in this region are very important.

All mixture fraction methods used here were based on complete equilibrium. While equilibrium can be a useful assumption in combustion systems, it might not be the best assumption to use in coal-based systems. Other such assumptions might include only products of complete combustion, or by substituting the water-gas shift reaction in place of complete equilibrium. It would be appropriate to test these different reaction assumptions using the mixture fraction methods discussed here in order to quantify any uncertainty in reaction assumptions, especially when applied to coal-based fuels.

4. Conclusions and Recommendations

The one-mixture fraction comparison showed that the NASA-CEA and Cantera equilibrium programs generally agree when using both simple hydrocarbon surrogate gases and more complex coal-based fuels. However, there was some significant deviation between the two programs with some of the high-rank coals (some anthracites and semi-anthracites) in very fuel-rich conditions ($\phi > 2$). These deviations occur due to the way Cantera was set up to handle unreacted fuel in order to minimize numerical instabilities in the equilibrium calculations. Both NASA and most of the Cantera equilibrium states convert the unreacted fuel to graphite, but in the few cases where deviation occurred, Cantera instead left the unreacted fuel with the same composition and properties of the original fuel. These deviations might be made smaller with improvements to the solid coal Cantera mechanism subroutine to better account for higher rank coals. While most industrial combustion applications do not use either high rank coals or such fuel-rich conditions on an overall basis, the local stoichiometry likely will fall to the fuel-rich extreme, especially in pyrolysis or gasification conditions. This means that more accurate modeling of fuel-rich conditions will be necessary for highly detailed, large-scale simulations of coal combustion systems.

In addition, the one-mixture fraction comparison showed that the equilibrium temperature and mole fractions of CO_2 and H_2O are highly dependent on the fuel used, and the CO mole fraction is highly dependent on the fuel only in fuel-rich conditions. In a one-mixture fraction system, this difference is nothing more than the difference in the elemental compositions of the original fuels, and this might be largely mitigated by using a combination of different surrogate gases and reference temperatures to match both composition and enthalpy of measured coal-based fuels. This procedure might cause the gas temperature to be out of the range of normal

990 combustion conditions or even to be an impossible temperature. However, using the surrogate
991 gases individually as direct replacements for coal-based fuels will make large-scale simulations
992 inaccurate for any combination of mixture fractions. This is especially true when trying to
993 accurately model gas compositions for radiative heat transfer calculations, which are greatly
994 influenced by both CO_2 and H_2O compositions. Not only do the gas compositions greatly affect
995 the heat transfer processes, but also impact many heterogeneous and homogenous reaction rates,
996 both in terms of actual reaction speed and diffusion speed. As a final note on the one-mixture
997 fraction analysis, the equilibrium oxygen content was not significantly influenced by fuel choice,
998 but more by the ratio of air to fuel. The oxygen content did not significantly change even for
999 coal-based fuels that can include a moderate amount of oxygen bound in the organic matrix.
1000 The two-mixture fraction comparison showed similar results to the one-mixture fraction
1001 approach for equilibrium temperature and mole fractions of CO_2, H_2O, and CO, especially in the
1002 limiting cases of using only one fuel. Both the CO and H_2O peak mole fractions varied by up to
1003 20 mol% based on fuel type, while the peak CO_2 mole fraction varied by closer to 10 mol%. The
1004 peak temperature varied between 2,200 and 2,400 K, depending on the fuel. In addition, the two-
1005 mixture fraction approach offers a broader range of values for the equilibrium temperature and
1006 mole fractions for the different combinations of component mixture fractions than the one-
1007 mixture fraction approach. While the two-mixture fraction approach does take more time, this
1008 approach is closer to what occurs in a real coal combustion system during devolatilization. The
1009 total volatiles enter the gas phase earlier than gases from the char reactions, and the tar and the
1010 light gases seem to be released at similar times in the pyrolysis process which is consistent with a
1011 two-mixture fraction approach. The O_2 mole fraction at equilibrium did not change much with
1012 respect to fuel choice in a manner similar to the one-mixture fraction approach. The peak O_2

mole fraction only varied by just over 0.2 mol% across all fuels in the two-mixture fraction comparison, with most of that variability in the coal surrogate fuels.

Both the one- and two-mixture fraction calculations showed that using measured coal-based fuel properties will always be more accurate than using coal surrogate gases (like graphite, benzene, methane, or other simple hydrocarbons or their combinations) as a direct substitution for coal-based fuels, especially in accurately modeling the CO_2, CO and H_2O mole fractions.

While the three-mixture fraction method offers a broader range of values in equilibrium temperatures and gas compositions than either the one- or two-mixture fraction methods, it is unclear whether a three-mixture fraction system is more realistic than a well-designed two-mixture fraction method. The two-mixture fraction method, if well designed, will allow for enough variability in fuel properties to come close to real coal reactions without adding too much complexity. Since the tar and light gases are released at similar times during coal pyrolysis, it is easy to justify a two-mixture fraction method, especially in simulations that do not have small enough time steps to differentiate between tar and light gas release. There is potential benefit, however, in using a three-mixture fraction approach in modeling coal combustion when trying to accurately model soot and soot precursors, since most of the soot in coal systems comes from the tar.

Acknowledgements

This work was supported in part by the Department of Energy, National Nuclear Security Administration, under Award Number DE-NA0002375.

References

[1] Smoot, L.D., Smith, P.J., Coal Combustion and Gasification, Plenum Press, New York, 1985.

[2] Chen, L., Yong, S.Z., Ghoniem, A.F., Oxy-Fuel Combustion of Pulverized Coal: Characterization, Fundamentals, Stabilization and CFD Modeling, Progress in Energy and Combustion Science, 2012;38:156-214.

[3] Pedel, J., Thornock, J.N., Smith, P.J., Ignition of Co-axial Turbulent Diffusion Oxy-coal Jet Flames: Experiments and Simulations Collaboration, Combustion and Flame, 2013;160:1112-1128.

[4] Smith, K.L., Smoot, L.D., Fletcher, T.H., Pugmire, R.J., The Structure and Reaction Processes of Coal, Plenum Press, New York, 1994.

[5] Barnhart, J.S., Laurendeau, N.M., Pulverized Coal Combustion and Gasification in a Cyclone Reactor .1. Experiment, Industrial & Engineering Chemistry Process Design and Development, 1982;21:671-680.

[6] Barnhart, J.S., Thomas, J.F., Laurendeau, N.M., Pulverized Coal Combustion and Gasification in a Cyclone Reactor .2. Model and Comparison With Experiment, Industrial & Engineering Chemistry Process Design and Development, 1982;21:681-689.

[7] Bhuiyan, A.A., Naser, J., Numerical Modelling of Oxy Fuel Combustion, the Effect of Radiative and Convective Heat Transfer and Burnout, Fuel, 2015;139:268-284.

[8] Bhunia, S., Sadhukhan, A.K., Haldar, S., Mondal, P.P., Prabhakar, A., Gupta, P., Devolatilization and Combustion of Coarse-Sized Coal Particles in Oxy–Fuel Conditions: Experimental and Modeling Studies, Energy & Fuels, 2018;32:839-854.

[9] Borghi, G., Sarofim, A.F., Beér, J.M., A Model of Coal Devolatilization and Combustion in Fluidized Beds, Combustion and Flame, 1985;61:1-16.

[10] Vascellari, M., Roberts, D.G., Hla, S.S., Harris, D.J., Hasse, C., From Laboratory-Scale Experiments to Industrial-Scale CFD Simulations of Entrained Flow Coal Gasification, Fuel, 2015;152:58-73.

[11] Rieth, M., Proch, F., Clements, A.G., Rabaçal, M., Kempf, A.M., Highly Resolved Flamelet LES of a Semi-Industrial Scale Coal Furnace, Proc. Combust. Inst., 2017;36:3371-3379.

[12] Wen, X., Luo, K., Wang, H.O., Luo, Y.J., Fan, J.R., Analysis of Pulverized Coal Flame Stabilized in a 3D Laminar Counterflow, Combustion and Flame, 2018;189:106-125.

[13] Backreedy, R.I., Habib, R., Jones, J.M., Pourkashanian, M., Williams, A., An Extended Coal Combustion Model, Fuel, 1999;78:1745-1754.

[14] Bradley, D., Lawes, M., Park, H.Y., Usta, N., Modeling of Laminar Pulverized Coal Flames With Speciated Devolatilization and Comparisons With Experiments, Combustion and Flame, 2006;144:190-204.

[15] Tufano, G.L., Stein, O.T., Kronenburg, A., Gentile, G., Stagni, A., Frassoldati, A., Faravelli, T., Kempf, A.M., Vascellari, M., Hasse, C., Fully-Resolved Simulations of Coal Particle Combustion Using a Detailed Multi-Step Approach for Heterogeneous Kinetics, Fuel, 2019;240:75-83.

[16] Van Essendelft, D., Li, T.W., Nicoletti, P., Jordan, T., Advanced Chemistry Surrogate Model Development within C3M for CFD Modeling, Part 1: Methodology Development for Coal Pyrolysis, Ind. Eng. Chem. Res., 2014;53:7780-7796.

[17] Fletcher, T.H., Hardesty, D.R., Compilation of Sandia Coal Devolatilization Data: Milestone Report, Sandia National Laboratories, Livermore, CA, 1992.

[18] Pielsticker, S., Gövert, B., Kreitzberg, T., Habermehl, M., Hatzfeld, O., Kneer, R., Simultaneous Investigation Into the Yields of 22 Pyrolysis Gases From Coal and Biomass in a Small-Scale Fluidized Bed Reactor, Fuel, 2017;190:420-434.

[19] Al-Abbas, A.H., Naser, J., Hussein, E.K., Numerical Simulation of Brown Coal Combustion in a 550 MW Tangentially-Fired Furnace Under Different Operating Conditions, Fuel, 2013;107:688-698.

[20] Costa, V.J., Krioukov, V.G., Maliska, C.R., Numerical Simulation of Pulverized Wet Coal Combustion Using Detailed Chemical Kinetics, J. Braz. Soc. Mech. Sci. Eng., 2014;36:661-672.

[21] Cui, K., Liu, B., Wu, Y.X., Yang, H.R., Lu, J.F., Zhang, H., Numerical Simulation of Oxy-coal Combustion for a Swirl Burner With EDC Model, Chin. J. Chem. Eng., 2014;22:193-201.

[22] Guo, J.J., Liu, Z.H., Wang, P., Huang, X.H., Li, J., Xu, P., Zheng, C.G., Numerical Investigation on Oxy-Combustion Characteristics of a 200 MW_e Tangentially Fired Boiler, Fuel, 2015;140:660-668.

[23] Hashimoto, N., Shirai, H., Numerical Simulation of Sub-Bituminous Coal and Bituminous Coal Mixed Combustion Employing Tabulated-Devolatilization-Process Model, Energy, 2014;71:399-413.

[24] Jovanovic, R., Milewska, A., Swiatkowski, B., Goanta, A., Spliethoff, H., Sensitivity Analysis of Different Devolatilisation Models on Predicting Ignition Point Position During Pulverized Coal Combustion in O_2/N_2 and O_2/CO_2 Atmospheres, Fuel, 2012;101:23-37.

1100 [25] Lisandy, K.Y., Kim, R.G., Hwang, C.W., Jeon, C.H., Sensitivity Test of Low Rank
1101 Indonesian Coal Utilization Using Steady State and Dynamic Simulations of Entrained-
1102 Type Gasifier, Appl. Therm. Eng., 2016;102:1433-1450.
1103 [26] Wen, X., Luo, K., Luo, Y.J., Kassem, H.I., Jin, H.H., Fan, J.R., Large Eddy Simulation of a
1104 Semi-Industrial Scale Coal Furnace Using Non-Adiabatic Three-Stream Flamelet/Progress
1105 Variable Model, Appl. Energy, 2016;183:1086-1097.
1106 [27] Watanabe, J., Okazaki, T., Yamamoto, K., Kuramashi, K., Baba, A., Large-Eddy Simulation
1107 of Pulverized Coal Combustion Using Flamelet Model, Proc. Combust. Inst.,
1108 2017;36:2155-2163.
1109 [28] Watanabe, J., Yamamoto, K., Flamelet Model for Pulverized Coal Combustion, Proc.
1110 Combust. Inst., 2015;35:2315-2322.
1111 [29] Rabaçal, M., Franchetti, B.M., Marincola, F.C., Proch, F., Costa, M., Hasse, C., Kempf,
1112 A.M., Large Eddy Simulation of Coal Combustion in a Large-Scale Laboratory Furnace,
1113 Proc. Combust. Inst., 2015;35:3609-3617.
1114 [30] Vascellari, M., Tufano, G.L., Stein, O.T., Kronenburg, A., Kempf, A.M., Scholtissek, A.,
1115 Hasse, C., A Flamelet/Progress Variable Approach for Modeling Coal Particle Ignition,
1116 Fuel, 2017;201:29-38.
1117 [31] Veras, C.A.G., Saastamoinen, J., Carvalho, J.A., Aho, N., Overlapping of the
1118 Devolatilization and Char Combustion Stages in the Burning of Coal Particles, Combustion
1119 and Flame, 1999;116:567-579.
1120 [32] Messig, D., Vascellari, M., Hasse, C., Flame Structure Analysis and Flamelet Progress
1121 Variable Modelling of Strained Coal Flames, Combust. Theory Model., 2017;21:700-721.

[33] Backreedy, R.I., Fletcher, L.M., Ma, L., Pourkashanian, M., Williams, A., Modelling Pulverised Coal Combustion Using a Detailed Coal Combustion Model, Combust. Sci. Technol., 2006;178:763-787.

[34] Franchetti, B.M., Marincola, F.C., Navarro-Martinez, S., Kempf, A.M., Large Eddy Simulation of a Pulverised Coal Jet Flame, Proc. Combust. Inst., 2013;34:2419-2426.

[35] Rebola, A., Azevedo, J.L.T., Modelling Pulverized Coal Combustion Using Air and O_2^+ Recirculated Flue Gas as Oxidant, Appl. Therm. Eng., 2015;83:1-7.

[36] Chen, L., Ghoniem, A.F., Simulation of Oxy-Coal Combustion in a 100 kW_{th} Test Facility Using RANS and LES: A Validation Study, Energy & Fuels, 2012;26:4783-4798.

[37] Theron, J.A., le Roux, E., Representation of Coal and Coal Derivatives in Process Modelling, Journal of the Southern African Institute of Mining and Metallurgy, 2015;115:339-348.

[38] Solomon, P.R., Fletcher, T.H., Pugmire, R.J., Progress in Coal Pyrolysis, Fuel, 1993;72:587-597.

[39] Fletcher, T.H., Review of 30 Years of Research Using the Chemical Percolation Devolatilization Model, Energy & Fuels, 2019;33:12123-12153.

[40] Richards, A.P., Johnson, C., Fletcher, T.H., Correlations of the Elemental Compositions of Primary Coal Tar and Char, Energy & Fuels, 2019;33:9520-9537.

[41] Goshayeshi, B., Sutherland, J.C., A Comparison of Various Models in Predicting Ignition Delay in Single-Particle Coal Combustion, Combustion and Flame, 2014;161:1900-1910.

[42] Xu, H.B., Hunger, F., Vascellari, M., Hasse, C., A Consistent Flamelet Formulation for a Reacting Char Particle Considering Curvature Effects, Combustion and Flame, 2013;160:2540-2558.

[43] Knappstein, R., Kuenne, G., Meier, T., Sadiki, A., Janicka, J., Evaluation of Coal Particle Volatiles Reaction by Using Detailed Kinetics and FGM Tabulated Chemistry, Fuel, 2017;201:39-52.

[44] Rieth, M., Kempf, A.M., Stein, O.T., Kronenburg, A., Hasse, C., Vascellari, M., Evaluation of a Flamelet/Progress Variable Approach for Pulverized Coal Combustion in a Turbulent Mixing Layer, Proc. Combust. Inst., 2019;37:2927-2934.

[45] Brewster, B.S., Baxter, L.L., Smoot, L.D., Treatment of Coal Devolatilization in Comprehensive Combustion Modeling, Energy & Fuels, 1988;2:362-370.

[46] Rieth, M., Proch, F., Rabaçal, M., Franchetti, B.M., Marincola, F.C., Kempf, A.M., Flamelet LES of a Semi-Industrial Pulverized Coal Furnace, Combustion and Flame, 2016;173:39-56.

[47] Wen, X., Luo, K., Jin, H.H., Fan, J.R., Numerical Investigation of Coal Flamelet Characteristics in a Laminar Counterflow With Detailed Chemistry, Fuel, 2017;195:232-242.

[48] Stollinger, M., Naud, B., Roekaerts, D., Beishuizen, N., Heinz, S., PDF Modeling and Simulations of Pulverized Coal Combustion - Part 1: Theory and Modeling, Combustion and Flame, 2013;160:384-395.

[49] Stollinger, M., Naud, B., Roekaerts, D., Beishuizen, N., Heinz, S., PDF Modeling and Simulations of Pulverized Coal Combustion - Part 2: Application, Combustion and Flame, 2013;160:396-410.

[50] Flores, D.V., Fletcher, T.H., The Use of Two Mixture Fractions to Treat Coal Combustion Products in Turbulent Pulverized-Coal Flames, Combust. Sci. Technol., 2000;150:1-26.

[51] Smoot, L.D., Pulverized Coal Diffusion Flames: A Perspective Through Modeling, Symposium (International) on Combustion, 1981;18:1185-1202.

[52] Radulovic, P.T., Ghani, M.U., Smoot, L.D., An Improved Model for Fixed Bed Coal Combustion and Gasification, Fuel, 1995;74:582-594.

[53] Tufano, G.L., Stein, O.T., Kronenburg, A., Frassoldati, A., Faravelli, T., Deng, L., Kempf, A.M., Vascellari, M., Hasse, C., Resolved Flow Simulation of Pulverized Coal Particle Devolatilization and Ignition in Air- and O_2/CO_2-Atmospheres, Fuel, 2016;186:285-292.

[54] Wen, X., Luo, Y.J., Wang, H.O., Luo, K., Jin, H.H., Fan, J.R., A Three Mixture Fraction Flamelet Model for Multi-Stream Laminar Pulverized Coal Combustion, Proc. Combust. Inst., 2019;37:2901-2910.

[55] Smith, P.J., Thomas H, F., Smoot, L.D., Model for Pulverized Coal-Fired Reactors, Symposium (International) on Combustion, 1981;18:1285-1293.

[56] Turns, S.R., An Introduction to Combustion: Concepts and Applications, 3rd ed., McGraw Hill, New York, 2012.

[57] Bilger, R.W., Conditional Moment Closure for Turbulent Reacting Flow, Physics of Fluids a-Fluid Dynamics, 1993;5:436-444.

[58] Bilger, R.W., Stårner, S.H., Kee, R.J., On Reduced Mechanisms for Methane-Air Combustion in Nonpremixed Flames, Combustion and Flame, 1990;80:135-149.

[59] Peters, N., Turbulent Combustion, Cambridge University Press, Cambridge, 2000, p.

[60] Fox, R.O., Computational Models for Turbulent Reacting Flows, Cambridge University Press, Cambridge, 2003.

[61] Poinsot, T., Veynante, D., Theoretical and Numerical Combustion, 2nd ed., Edwards, Philadelphia, 2005.

[62] Gordon, S., McBride, B.J., Computer Program for Calculation of Complex Chemical Equilibrium Compositions and Applications I. Analysis., NASA RP 1311, NASA, USA, 1994.

[63] McBride, B.J., Gordon, S., Computer Program for Calculation of Complex Chemical Equilibrium Compositions and Applications II. Users Manual and Program Description., NASA RP 1311, NASA, USA, 1996.

[64] Goodwin, D.G., Speth, R.L., Moffat, H.K., Weber, B.W., Cantera: An object-oriented software toolkit for chemical kinetics, thermodynamics, and transport processes, Version 2.4.0, 2018, https://www.cantera.org.

[65] Richards, A.P., Haycock, D., Frandsen, J., Fletcher, T.H., A Review of Coal Heating Value Correlations With Application to Coal Char, Tar, and Other Fuels, Fuel, 2021;283:118942.

[66] Green, D.W., Perry's Chemical Engineers' Handbook, in, McGraw Hill, New York, 1984.

[67] Proscia, W.M., Freihaut, J.D., Rastogi, S., Klinzing, G.E., Thermodynamic Properties of Pulverized Coal During Rapid Heating Devolatilization Processes, DOE/PC/92176—T8, R. Center, United States Office of the Assistant Secretary for Fossil Energy, USDOE, East Hartford, Connecticut (United States), U.T. Corporation, 1994.

[68] Edwards, J.H., Smith, I.W., Tyler, R.J., CSIRO Flash Pyrolysis Project: Compendium of Data, Commonwealth Scientific and Industrial Research Organization, North Ryde (Australia). Div. of Fossil Fuel, 1983.

[69] Miller, B.G., 1 - The Chemical and Physical Characteristics of Coal, in: Clean Coal Engineering Technology (Second Edition), Butterworth-Heinemann, 2017, pp. 3-60.

[70] Richards, A.P., Coal Pyrolysis Models for Use in Massively Parallel Oxyfuel-Fired Boiler Simulations, Dissertation, Chemical Engineering, Brigham Young University (in preparation, 2020).

[71] Brown, A.L., Modeling Soot in Pulverized Coal Flames, Masters, Mechanical Engineering, Brigham Young University (1997).

[72] Josephson, A.J., Gaffin, N.D., Smith, S.T., Fletcher, T.H., Lignell, D.O., Modeling Soot Oxidation and Gasification with Bayesian Statistics, Energy & Fuels, 2017;31:11291-11303.